Lattice Differential Operators for Computational Physics

A Thesis
Submitted for the Degree of
Master of Science (Engineering)

by

Rashmi Ramaadugu

Engineering Mechanics Unit
Jawaharlal Nehru Centre for Advanced Scientific Research
(A Deemed University)
Bangalore – 560 064

JANUARY 2014

To my father Late Sri. R. Someswar Rao

DECLARATION

I hereby declare that the matter embodied in the thesis entitled "**Lattice Differential Operators for Computational Physics**" is the result of investigations carried out by me as a student of the Engineering Mechanics Unit, Jawaharlal Nehru Centre for Advanced Scientific Research, Bangalore, India under the supervision of **Dr. Santosh Ansumali** and that it has not been submitted elsewhere for the award of any degree or diploma.

In keeping with the general practice in reporting scientific observations, due acknowledgment has been made whenever the work described is based on the findings of other investigators.

Rashmi Ramaadugu

CERTIFICATE

I hereby certify that the matter embodied in this thesis entitled "**Lattice Differential Operators for Computational Physics**" has been carried out by **Mrs. Rashmi Ramaadugu** as a student of the Engineering Mechanics Unit, Jawaharlal Nehru Centre for Advanced Scientific Research, Bangalore, India under my supervision and that it has not been submitted elsewhere for the award of any degree or diploma.

Dr. Santosh Ansumali
(Research Supervisor)

Acknowledgements

I cherish the moments I spent in EMU throughout my life. I would like to first acknowledge my gratitude to my advisor *Dr. Santosh Ansumali* for his constant support, motivation and opportunities to work on various areas. I thank my collaborators *Prof. Sauro Succi, Prof. Ronojoy Adhikari* and *Dr. Sumesh Thampi* for their guidance and inspiration. I thank *Sumesh* for answering all my queries patiently. I thank *Prof. KR Sreenivas* for teaching Heat Transfer and giving me opportunity to setup and experiment on *"Tears of Wine"*. I thank *Prof. Ganesh Subramaniam* for teaching Fluid Mechanics. I thank *Prof. Rama Govindarajan* for teaching Mathematical methods and inspirational lectures. I thank *Prof. Mehboob Alam* for teaching Thermodynamics and Brownian Motion. I thank *Prof. V. Kumaran* for teaching Physics of fluids and *Prof Umesh Waghmare* for his motivation.

It was fun working with my lab mates *Chakradhar, Manjusha, Shivani, Siddarth, Reddy, Vicky, Shajahan* where I got relieved of the stress. I thank *Deepthi* for the combined studies and motivation during hard times. I thank *Ponnu* for mentoring me. I thank my batchmates *Deepak, Kanwar, Saikat, Ramakrishna* for all their help and fun we had together after exams. I thank *Shasank, Vaibhav* and *Mamtha* for helping me in *"Tears of Wine"* experiment. I thank all the EMU mates *Jose, Prashant, Rajesh, Sankalp, Navneet, Sunil, Saikishan, Aarti, Croor, Reddy. Jr* for all their help.

I thank my parents *(Late. R. Someswar Rao and R. Saraswathi)* and sister *(Dr. Sneha Lakshmi)* for motivating me from my childhood. I thank my husband *Anil* for all the co-operation. I thank my beloved kids *(Aarush and Ayanesh)* for their love. I thank the admin staff *Sukanya, Princy, Vijaya Lakshmi, Gayathri* for making my stay at EMU a pleasant one.

Abstract

Differential operators such as gradient, curl, laplacian and divergence used in vector algebra follow certain identities and symmetries, which often is absent in their discrete counterpart. For example, the laplacian operator is rotationaly symmetric. The aim of the present work is to present a general procedure to derive second order accurate discrete operators, which are isotropic to the leading order. Furthermore, by taking advantage of isotropic nature of leading order error in discrete operator, a recursive technique is developed to increase the order of accuracy of the operator.

In order to derive discrete operators with necessary isotropy, general discrete operators on arbitrary space-filling lattice are considered. It has been shown that the problem of preserving isotropy of the continuous operator in their discrete counterpart can be mapped to problem of finding discrete analog of Maxwell-Boltzmann distribution. This information is used to find a set of discrete operators which are isotropic to the leading orders. Furthermore, it is shown that widely used concept of staggered grid can be changed to replica grid and combined with current procedure to find highly accurate discrete operators.

In order to illustrate the power of current technique various applications are considered. In particular, as a first example current technique is applied to wave equation and is contrasted with standard finite difference methods. As electrodynamics based on current formulation of solving wave equations, an isotropic extension of Yee method of solving Maxwell equation is constructed. Finally, an isotropic version of the standard Maccormack method is discussed.

List of Figures

List of Tables

Contents

Chapter 1

Introduction

Introduction

Lower order finite difference methods(LeVeque 2007; Chung 2010) remain one of the best option for discretizing the differential operators because of their ease of implemenation for complex geometries. But the accuracy of these lower order methods is very poor compared to the spectral methods(Trefethen 1996; Canuto *et al.* 2007). Accuracy of the finite difference schemes can be improved by increasing the stencil size. In general, all the finite difference are formulated for one dimension and the same is extended to the multi-dimensions(Lele 1992; Tam & Webb 1993). By doing so, the operator is restrained to principal directions only and all the other grid points are neglected. This leads to loss of isotropy, which is an inherent property of continuum space. This inabliity of the operators may reflect in the numerical simulations of the physical problems. It is therefore desirable that discrete versions retain all the symmetries of their continuum counterparts. This issue was addressed previously by many via mimetic discretizations(Bochev & Hyman 2006; Hyman & Shashkov 1999), compact discretizations(Lele 1992; Kim & Lee 1996) and dispersion preserving discretizations(Cheong & Lee 2001; Zhuang & Chen 1998; Tam & Webb 1993). With specific regard to isotropy there are few works in the past(Patra & Karttunen 2006; Kumar 2004; Thampi *et al.* 2012) but they are restrained to the isotropy of the laplacian operator only (Thampi *et al.* 2012).

In this thesis, we derived general discrete opeartors from a generating function which enables the formulation of the discrete operators such as curl, divergence, gradient and laplacian.The isotropy of these operators is ensured by taking the constraints analogous to finding the discrete velocity sets and their associated Maxwell-Boltzmann equillibrium distributions from the lattice kinetic theory.A recursive technique to improve the order of accuarcy is discussed. We then generalize the concept of staggered grid to that of replica grid, where multiple copies of space filling lattices are introduced simultanously. These grids are obtained via translation of original grid by fixed amount and unlike staggered grid formulations, all variables are kept on all grids. These operators are used on both the single grid and replica grid and the various Time-dependent linear partial differential equation (hereafter PDE) such as advection, diffusion and wave equations are compared with the standard central difference operators. The isotropic discretization of the Maxwell equations is done using the replica schemes and compared with the standard yee scheme(Yee 1966).

The organization of the thesis is as follows:

- **Chapter. 2:** The formulation of general discrete operator from a generating function is discussed. Further recursive technique used to develop fourth order scheme and the concept of replica grid is introduced.

- **Chapter. 3:** The discrete operators are applied to obtain numerical schemes for various PDEs such as the advection, diffusion, wave and Maxwell equations. The consequence of having discrete isotropy is analysed via dispersion relation.
- **Chapter. 4:** A brief summary and conclusions for the present thesis is given in this chapter.

Chapter 2
Lattice Differential Operators

2.1 Introduction

Discrete operations(Taflove & Hagness 2000; Laney 1998) are generally restrained to the principal directions of the lattice (coordinate directions on a rectangular grid), often neglecting the grid points along other directions (Alford *et al.* 1974). This leads to a loss of information about phase which deteriorates the accuracy of the discrete operation, isotropy in the first place. This inability to perform discrete operations satisfying the inherent isotropy of continuum space may reflect severely on numerical simulations of physical problems. It is therefore desirable to develop discrete operators which retain as many symmetries as possible of their continuum counterparts.

Furthermore, a major disadvantage of the typical higher order finite difference approaches is wider stencil sizes as the order of the approximation is increased. These large stencils tends to be cumbersome near the edge of the domain where no data is available to perform the differencing. In last few decade, finite differences with narrower stencil and higher order accuracies are obtained via implicit differencing schemes Lele (1992). These implicit difference schemes rely on Taylor series representation and typically they are formulated in one dimensional sense only.

In this chapter, we show that the problem of finding discrete operators which respect isotropy and symmetries of the continuous operator is analogous to finding discrete velocity models for which lower order moments of discrete equilibrium matches with that of Maxwell-Boltzmann distribution. We also show that compact finite difference schemes can be formulated directly in multidimensional sense, provided the leading order error in discrete operators are isotropic. We also suggest an explicit formulation which is computationally more advantageous than implicit form.

Finally, we generalize the concept of staggered grid to that of replica grid, where multiple copies of space filling lattices are introduced simultaneously. These grids are obtained via translation of original grid by fixed amount and unlike staggered grid formulations, all variables are kept on all grids. We show that such replica grids coupled with isotropic operators provide an efficient alternate to existing finite difference methods.

The chapter is organized as follows: Sec. 2.2 and 2.3, briefly discusses the pertinent symmetry and isotropy of differential operators and evaluates a few existing schemes from the point of view of the rotational invariance. In Sec. 2.4, the formulation of general operator on a lattice is discussed along with the review of the constraints from the kinetic theory. Sec. 2.5, discusses the formulation of the operator using a generating function and in Sec. 2.6, the refinement for the proposed scheme to get a fourth order scheme is discussed. Sec. 2.7, discusses the isotropy using green's function and fourier analysis and validation of the proposed schemes with testcases.

2.2 Discrete Operator and Symmetry

In this section, we highlight how some of the basic continuous symmetry get violated in discrete case. In order to illustrate this aspect, we consider the laplacian as an example where loss of isotropy in discrete case is quite apparent.

For example, if we consider a rotation of coordinate axis $x_i' = A_{ik}x_k$, characterized by an orthogonal $n \times n$ matrix A, the gradient operator transforms as:

$$\frac{\partial}{\partial x_i} = A_{ik}\frac{\partial}{\partial x_k'}. \tag{2.1}$$

It can be seen from the relation

$$\nabla_i^2 = A_{ij}A_{ik}\frac{\partial^2}{\partial x_j'\partial x_k'} = \nabla_i'^2 \tag{2.2}$$

that such a transformation, leaves laplacian invariant. This invariance is more explicit in the fourier domain, where we can see that the fourier transform of the laplacian $\mathcal{L}(\mathbf{k}) = -k^2$, is only a function of the magnitude of the wavenumber. A consequence of this isotropy is that the laplacian of a radial function remains radial. For example, in 2-Dimension, the Green function for laplace equation is $f(x, y) = (log|r|)/(2\,\pi)$, for which

$$\nabla^2 f(\mathbf{r}) = \delta(0). \tag{2.3}$$

It is desirable that when laplace operator is discretized, this isotropy of the laplace operator is retained. To be more precise, one would like to have fourier transform of the discrete laplacian $\tilde{\mathcal{L}}(\mathbf{k})$ is such that the error$\tilde{\mathcal{L}}(\mathbf{k}) - \mathcal{L}(\mathbf{k})$ is only a function of k at least for the leading order term.

At this point, we remind the reader that one of the simplest approximation to the laplacian, often used in numerical simulation is discrete laplacian obtained via central difference operator for derivative defined as

$$\frac{d^2 f}{dx^2} \approx \frac{f(x + \Delta x) + f(x - \Delta x) - 2f(x)}{\Delta x^2}. \tag{2.4}$$

As an example, the discrete laplacian $\widetilde{\nabla}^2$ of a scalar field $f(x, y)$ using standard central difference of second order in 2D at (i, j) point in space is often given as

$$\widetilde{\nabla}^2 f_{i,j} = \frac{f_{i+1,j} - 2f_{i,j} + f_{i-1,j}}{c^2} + \frac{f_{i,j+1} - 2f_{i,j} + f_{i,j-1}}{c^2}, \tag{2.5}$$

where c is the grid spacing and $f_{i,j}$ is the value of f at (i, j) point in space (See Fig. (2.1)).

It can be seen via Taylor series expansion that discrete laplacian approximate the continuous laplacian as

$$\widetilde{\nabla}^2 \approx \nabla^2 + \frac{c^2}{12}\left(\frac{\partial^4}{\partial x^4} + \frac{\partial^4}{\partial y^4}\right). \tag{2.6}$$

In this expression, it is quite evident that the leading order error is anisotropic. This is also

evident in the fourier space where we see that the fourier transform of the discrete laplacian

$$\tilde{\mathcal{L}}(\mathbf{k}) = \mathcal{L}(\mathbf{k}) + \frac{c^2}{12}k^4\left(1 - 2\cos^2\theta\sin^2\theta\right), \tag{2.7}$$

has angular dependence.

Furthermore, we can also note that the radial nature of the model function $f(x, y) = \ln(r), r = \sqrt{x^2 + y^2}$ is not preserved by discrete laplacian of it

$$\widetilde{\nabla^2} f = \frac{c^2}{r^4}\left(7 - 16\cos^2\theta\sin^2\theta\right). \tag{2.8}$$

It is evident from the Fig. 2.2 and Fig. 2.3, that the error in case of the central difference laplacian is not isotropic. The error is not the same at all angles which shows the angular dependence of the central difference operator.

It can therefore be concluded that the conventional method of constructing the laplacian via taking central difference operator in each of the dimension separetely is not isotropic.

2.3 Generators for Differential Operators

The goal of this thesis is to develop a discrete analog of operators defined in vector analysis on a Cartesian grid. Before doing so, in this section we briefly remind the reader about basic definitions of vector operators and associated structural properties, which one would like to preserve on the grid. A few important operators, which we shall define on the grid, are gradient, divergence, curl and laplacian operators. In the following, we shall show that all of the above mentioned operators appears naturally from a generator. As an example, for any scalar function $\psi(\mathbf{x})$, an infinitely small parallel displacement over a distance $d\mathbf{x}_i$ acts as the generator of the gradient operator. This can be seen from the relation

$$\psi(\mathbf{x} + d\mathbf{x}) \approx \psi(\mathbf{x}) + dx_i\nabla_i\psi, \tag{2.9}$$

which leads to a generic definition of the gradient operator independent of the co-ordinate system (Griffiths & College 1999)Similarly, a generic definition of divergence operator acting on a vector field $\mathbf{u}$ is obtained via Guass theorem as

$$\int_v \boldsymbol{\nabla}\cdot\mathbf{u}d\tau = \oint_s \mathbf{u}\cdot d\mathbf{a}, \tag{2.10}$$

$$\oint_s (\boldsymbol{\nabla}\times\mathbf{u})\cdot d\mathbf{a} = \oint \mathbf{u}\cdot d\mathbf{l}. \tag{2.11}$$

where $d\mathbf{a}$, $d\mathbf{l}$ and $d\tau$ are infinitely small area, length and volume elements respectively . Typically, one start with these definitions for creating discrete operators Hyman & Shashkov (1999). However, in this thesis we shall take an alternate route, where we convert a given differential operator into an integral operator. For example, we can introduce integral form for gradient as

$$\nabla_i\psi(\mathbf{r}) = \int d\mathbf{x}\delta(\mathbf{x} - \mathbf{r}), \frac{\partial\psi(\mathbf{x})}{\partial x_i}, \tag{2.12}$$

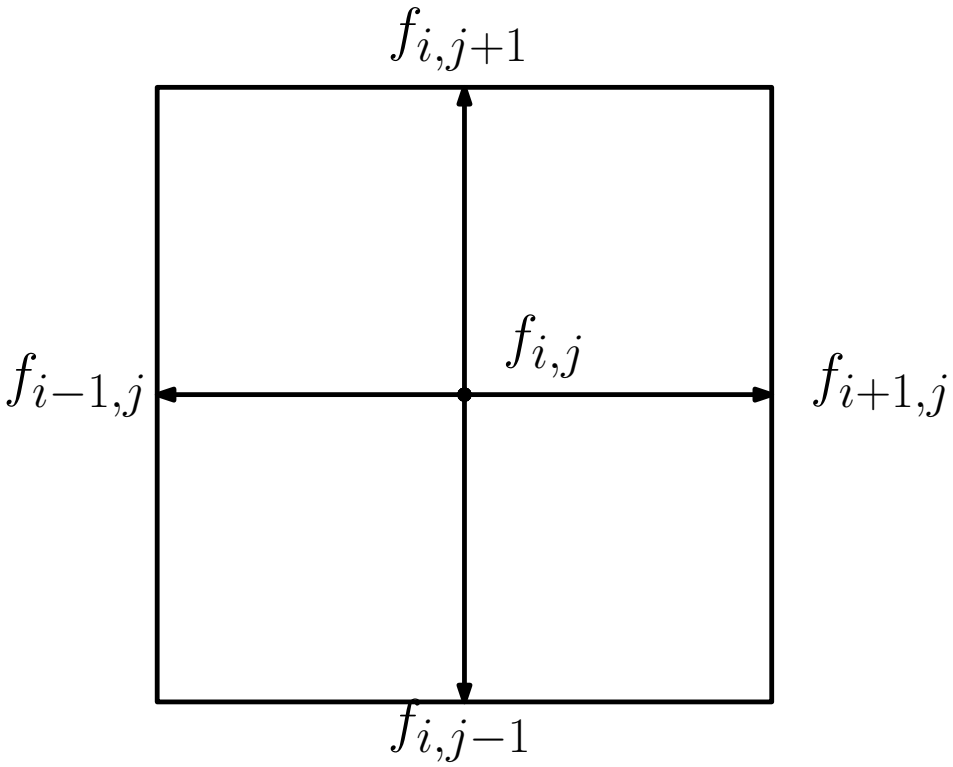

Figure 2.1: 2D stencil for Central Difference(CD2) operator.

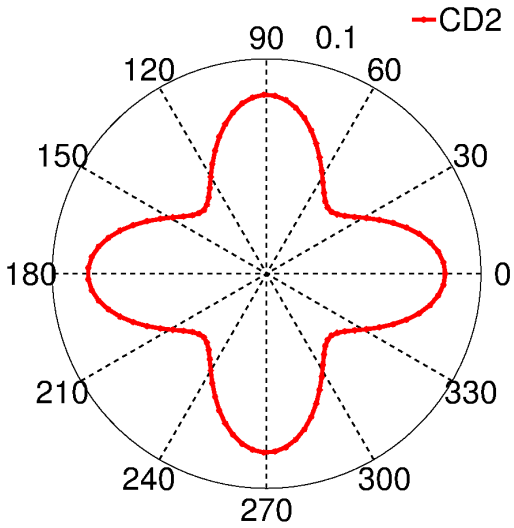

Figure 2.2: Polar plot of Eq. 2.7. Here the radius of the plot represents the normalized error (i.e) $\frac{\tilde{\mathcal{L}}(\mathbf{k})-\mathcal{L}(\mathbf{k})}{k^4c^2}$.

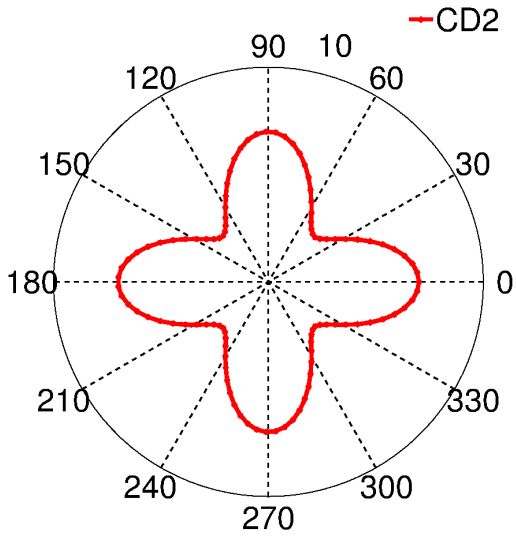

Figure 2.3: Polar plot of Eq. 2.8. Here the radius of the plot represents the normalized error.

which upon integrating by parts can be re-written as:

$$\nabla_i \psi(\mathbf{r}) = -\int d\mathbf{x} \psi(\mathbf{x}) \frac{\partial \delta(\mathbf{x}-\mathbf{r})}{\partial x_i}. \tag{2.13}$$

Via this alternate representation, we have achieved our goal of representing differential operators to an integral operator. At this point, we would like to represent it in a form convenient for numerical evaluation on a grid. If we consider, the sequence of family of Guassian functions in D-dimension

$$\delta_\epsilon(\mathbf{r}) = \left(\frac{1}{\sqrt{2\pi\epsilon}}\right)^D \exp\left(-\frac{y^2}{2\epsilon}\right), \tag{2.14}$$

the Dirac delta function emerges as the limit $\lim_{\epsilon\to 0^+} \delta_\epsilon(\mathbf{r})$. With this simplification, Eq. 2.13 can be rearranged to write the gradient operator as

$$\nabla_i \psi(\mathbf{r}) \equiv \left[\left(\frac{1}{\sqrt{2\pi\epsilon}}\right)^D \int d\mathbf{y} \exp\left(-\frac{y^2}{2\epsilon}\right) \frac{y_i}{\epsilon} S_\mathbf{y}\right] \psi(\mathbf{r}), \tag{2.15}$$

where $S_\mathbf{y}$ defined as

$$S_\mathbf{y} \psi(\mathbf{r}) = \psi(\mathbf{y}+\mathbf{r}), \tag{2.16}$$

is the standard shift operator emerging due to space translation. A very similar analysis on divergence and curl operator shows that

$$\nabla_i u_i(\mathbf{r}) \equiv \left[\left(\frac{1}{\sqrt{2\pi\epsilon}}\right)^D \int d\mathbf{y} \exp\left(-\frac{y^2}{2\epsilon}\right) \frac{y_i}{\epsilon} S_\mathbf{y}\right] u_i(\mathbf{r}), \tag{2.17}$$

$$\boldsymbol{\nabla}\times\mathbf{u}(\mathbf{r}) \equiv \left[\left(\frac{1}{\sqrt{2\pi\epsilon}}\right)^D \int d\mathbf{y} \exp\left(-\frac{y^2}{2\epsilon}\right) \frac{1}{\epsilon}\mathbf{y}\times S_\mathbf{y}\right] \mathbf{u}(\mathbf{r}). \tag{2.18}$$

Any second order operators such as laplacian can always be constructed via appropriate first order operators (for example $\nabla^2 \equiv \nabla_i \nabla_i$). However, it is often convenient to construct the

laplacian directly. Thus, following route of replacing differential operator with that of integral operators, laplacian can always be written as

$$\nabla^2 \mathbf{u}(\mathbf{r}) \equiv \left[\left(\frac{1}{\sqrt{2\pi\epsilon}} \right)^D \int d\mathbf{y} \exp\left(-\frac{y^2}{2\epsilon} \right) \left(\frac{y_i^2}{\epsilon^2} - 2 \right) \times S_{\mathbf{y}} \right] \mathbf{u}(\mathbf{r}). \tag{2.19}$$

It should be noted that the form of these operators Eq.2.15 are now quite convienent for numerical integration via Gauss-Hermite quadrature. Furthermore, all of these operators can be derived via a single generator

$$G \equiv \left(\frac{1}{\sqrt{2\pi\epsilon}} \right)^D \int d\mathbf{y} \exp\left(-\frac{y^2}{2\epsilon} \right) \exp\left(y_i \, s_i \right), \tag{2.20}$$

by taking appropriate derivative with respect to $s_i \equiv \nabla_i$. For later analysis, it would be convenient to highlight, the differential form of the operator obtained via Guassian integration, as

$$G\left[\psi(\mathbf{r})\right] = \left(1 + \frac{\epsilon}{2} \nabla^2 + \frac{\epsilon^2}{8} \nabla^4 + \cdots \right) \psi(\mathbf{r}), \tag{2.21}$$

which shows that operator G is isotropic. Later, we shall use this expression to get discrete version of the operator.

2.4 General Operator on a Lattice

In this section, we shall construct a general procedure to derive operators on a lattice, which can preserve isotropy to the desired accuracy. We remind the reader that a lattice may be viewed as a regular tiling of a space by a primitive cell. Thus, any given lattice can be parameterized by the set of link vectors $\mathbf{e}_i \in \mathcal{C}$, where $\mathbf{e}_i$ denotes the translation of unit cellwhich will map the lattice onto itself.

Notice that the discrete generator is an operator and only its action of a function is integral, thus a straight forward application of Guassian quadrature cannot be done. We begin by noting that on a lattice, a Gaussian quadrature type formulation can be used to approximate the generator in Eq. 2.20 as

$$\tilde{G}\left[\phi(\mathbf{r})\right] \equiv \sum_i w_i \exp(y_i s_i) \phi(\mathbf{r}) = \sum_i w_i \phi(\mathbf{r} + \mathbf{e}_i), \tag{2.22}$$

where w_i denotes weights associated with each of the connector direction. The action of this discrete generator on any function $\psi(\mathbf{r})$ is:

$$\begin{aligned} \tilde{G}\left[\psi(\mathbf{r})\right] = \Bigg[\sum_i w_i + \left(\sum_i w_i e_{i\alpha} \right) \frac{\partial}{\partial r_\alpha} + \frac{\sum_i w_i e_{i\alpha} e_{i\beta}}{2} \frac{\partial^2}{\partial r_\alpha \partial r_\beta} \\ + \frac{\sum_i w_i e_{i\alpha} e_{i\beta} e_{i\gamma}}{6} \frac{\partial^3}{\partial r_\alpha \partial r_\beta \partial r_\gamma} + \frac{1}{24} \left(\sum_i w_i e_{i\alpha} e_{i\beta} e_{i\gamma} e_{i\kappa} \right) \frac{\partial^4}{\partial r_\alpha \partial r_\beta \partial r_\gamma \partial r_\kappa} + \cdots \Bigg] \psi(\mathbf{r}), \end{aligned} \tag{2.23}$$

Here, we would follow a procedure similar to quadrature derivation (Arfken *et al.* 2005),

where we require that discrete and continuous operator Eq. 2.23 and Eq. 2.21 leads to same action on polynomials of increasing order. Following (Yudistiawan *et al.* 2010) we firsly link accuracy requirement with the closure properties of the chosen lattice as follows:

- **Normalization Condition:** We would like that the action of discrete generator and continuous generator are identical for a constant scalar field $\psi(r) = 1$. Thus, using Eq. 2.23 and Eq. 2.21, we have the normalization condition:

$$\sum_i w_i = 1. \tag{2.24}$$

- **Closure under Inversion:** At this point, if we invoke the argument of spatial isotropy and demand that weight $w(\mathbf{e}_i)$ is a function of magnitude of $\mathbf{e}$ only i.e., $w(\mathbf{e}_i) = w(e_i^2)$, the condition that discrete operator is exact for the linear polynomial $\psi(r) = a_\alpha r_\alpha$ using Eq. 2.23 and Eq. 2.21, reduces to

$$\sum_i w_i e_{i\alpha} = 0. \tag{2.25}$$

  This implies that for any connectivity vector $\mathbf{e_i}$ is an element of the set $\mathcal{C}$ then the inverse of the it also exists in the same set (i.e),

$$\mathbf{e}_i \in \mathcal{C} \Longleftrightarrow -\mathbf{e}_i \in \mathcal{C}. \tag{2.26}$$

  Using these conditions, Eq. 2.23, simplifies as

$$\begin{aligned}\tilde{G}\left[\psi(\mathbf{r})\right] = G\left[\psi(\mathbf{r})\right] + \Bigg[\frac{1}{2}\left(\sum_i w_i e_{i\alpha} e_{i\beta} - \epsilon\delta_{\alpha\beta}\right)\frac{\partial^2}{\partial r_\alpha \partial r_\beta} \\ + \frac{1}{24}\left(\sum_i w_i e_{i\alpha} e_{i\beta} e_{i\gamma} e_{i\kappa} - \epsilon^2 \Delta_{\alpha\beta\gamma\theta}\right)\frac{\partial^4}{\partial r_\alpha \partial r_\beta \partial r_\gamma \partial r_\kappa}\Bigg]\psi(\mathbf{r}),\end{aligned} \tag{2.27}$$

  where $\Delta_{\alpha\beta\gamma\theta} = \delta_{\alpha\beta}\delta_{\gamma\theta} + \delta_{\alpha\gamma}\delta_{\beta\theta} + \delta_{\alpha\theta}\delta_{\beta\gamma}$ and we have used the fact that closure under inversion also imply

$$\sum_i w_i e_{i\alpha} e_{i\beta} e_{i\gamma} = 0. \tag{2.28}$$

- **Closure under Reflection:** Next, we would like the discrete operator Eq. 2.27 to be exact for a general quadratic polynomials $a_{\alpha\beta} r_\alpha r_\beta$. Then, we have from Eq. 2.21 and Eq. 2.27 that

$$\sum_i w_i e_{i\alpha} e_{i\beta} = \epsilon\delta_{\alpha\beta}. \tag{2.29}$$

  This implies that for a connectivity vector $\mathbf{e}_i$ is an element of set $\mathcal{C}$, all possible reflections

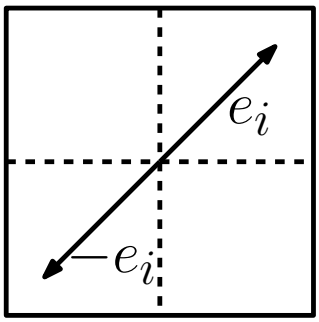

Figure 2.4: Illustration of closure under inversion. Here e_i represents the connectivity vector and $-e_i$ represents the inverse of the original connectivity vector.

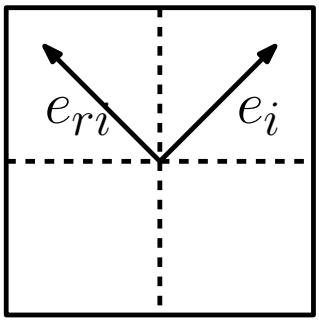

Figure 2.5: Illustration of closure under reflection. Here e_i represents the connectivity vector and e_{ri} represents the reflection of the original connectivity vector.

of it (i.e) $(\pm e_{ix}, \pm e_{iy}, \cdots)$ also exists in the same set $\mathcal{C}$, (i.e),

$$\mathbf{e}_i \in \mathcal{C} \Longleftrightarrow (\pm e_{ix}, \pm e_{iy}, \cdots) \in \mathcal{C} \tag{2.30}$$

which is shown in the Fig. 2.5.

This condition also implies in 3-Dimension that:

$$\sum_i w_i e_{ix}^{2\,m} = \sum_i w_i e_{iy}^{2\,m} = \sum_i w_i e_{iz}^{2\,m}, \tag{2.31}$$

for any integer m.

- **Fourth Order Isotropy**: A similar calulation for arbitrary fourth order polynomial will imply that if we can ensure that

$$\sum_i w_i \mathbf{e}_{i\alpha}\mathbf{e}_{i\beta}\mathbf{e}_{i\gamma}\mathbf{e}_{i\theta} \quad = \quad \epsilon^2 \Delta_{\alpha\beta\gamma\theta}, \tag{2.32}$$

then continuous and discrete operators will match for any fourth order polynomial.

In Fig. 2.6, three space filling lattices which wil satisfy the above mentioned constraints of closure under inversion and reflection in 2-Dimension is shown. The second lattice is obtained from the first one via a rotation of $\pi/4$. While first and third space filling lattice (Fig. (a) and Fig. 2.6) is used in central difference operator, either third lattice or a union of the first two lattices is commonly used in the lattice Boltzmann approach Succi (2001).

2.4.1 Search for Optimal Grid and Associated Weights

As mentioned above, if discrete generator is fourth order accurate it has to satify a number of constraints given by Eqs.2.25,2.29,2.28,2.32. Using closure under inversion and reflection, these constraints simplifies to:

$$\begin{aligned} \sum_i w_i &= 1, \\ \sum_i w_i c_{ix}^2 &= \epsilon, \\ \sum_i w_i c_{ix}^4 &= 3\,\epsilon^2, \\ \sum_i w_i c_{ix}^2\, c_{iy}^2 &= \epsilon^2. \end{aligned} \tag{2.33}$$

It is easy to check in general that it is not possible to satisfy Eq.2.33 with a basic lattices alone Thus, in the lattice Boltzmann approach, where exactly same conditions is imposed on the lattice in the velocity space, a concept of union lattice is introduced. In this approach, two seperate lattices are superimposed on each other in such a way that Eq.2.33 is satisfied while space-filling property is preserved for numerical convenience as shown in Fig. 2.7. Hereafter, we borrow LB terminology of denoting n point stencil scheme in m dimension as DnQm lattice and denoting elementary lattices where on a given lattice c_i^2 = constant as energy shells (Yudistiawan *et al.* 2010; Chikatamarla & Karlin 2009).

As for example, if we take a union of square lattice with spacing $\Delta x = \Delta y = c$ and its rotation by $\pi/4$, we have a set of four equation for w_0, w_1, w_2 and ϵ:

$$\begin{aligned} w_0 + 4\,w_1 + 4\,w_2 &= 1, \\ 2\,w_1 + 4\,w_2 &= \frac{\epsilon}{c^2}, \\ 2\,w_1 + 4\,w_2 &= \frac{3\,\epsilon^2}{c^4}, \\ 4\,w_2 &= \frac{\epsilon^2}{c^4}. \end{aligned} \tag{2.34}$$

This set of equation can be inverted to obtain the weights and spacing c for D2Q9 lattice as:

$$w_0 = \frac{16}{36}, \quad w_1 = \frac{4}{36}, \quad w_2 = \frac{1}{36}, \quad \epsilon = \frac{c^2}{3}. \tag{2.35}$$

The same process can be repeated in $3-D$ and the weights of the standard models (provide figure for different 3-D lattices) are given in the Table. 2.1 Thampi *et al.* (2012); Ramadugu *et al.* (2013).

There is no fundamental reason that a union stencil should only be constructed by superimposing two elementary lattices on same grid with same spacing, but the only constraint which should be satisfied is that the union of the two elementary lattice should also form a regular tiling of the space. As an example in 2D, if we take a lattice constructed by elementary lattices shown in Fig. 2.6 (a) and introduce a space translation by amount $(\Delta x/2, \Delta x/2)$, we have a composite space filling lattice structure as shown in Fig. 2.8. Notice that while original lattice

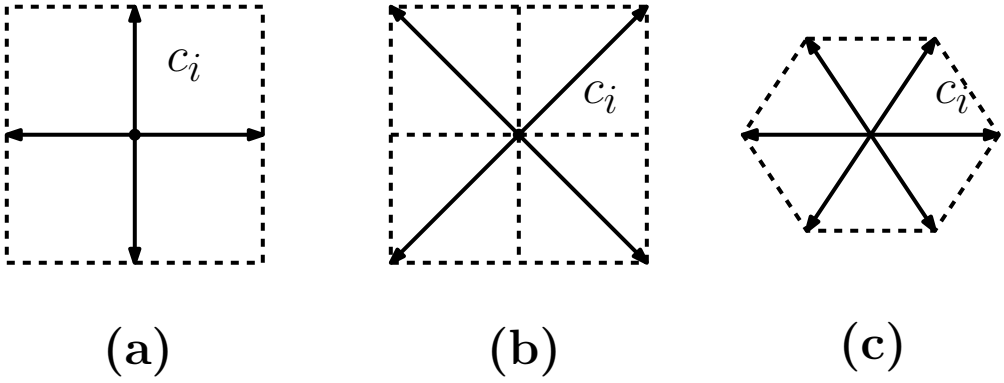

Figure 2.6: 2D grid with all possible connectivity vectors e_i.

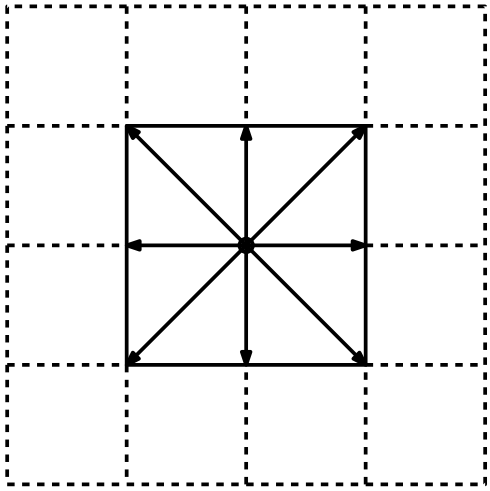

Figure 2.7: D2Q9 lattice model on a simple 2D grid.

	N,	(for 2D)	D2Q9	D3Q15	D3Q19	D3Q27
0	1	(1)	4/9	2/9	1/3	8/27
NN	6	(4)	1/9	1/9	1/18	2/27
NNN	12	(4)	1/36	0	1/36	1/54
NNNN	8	(0)	0	1/72	0	1/216

Table 2.1: Popular DnQm models and their weights along with the values of N.

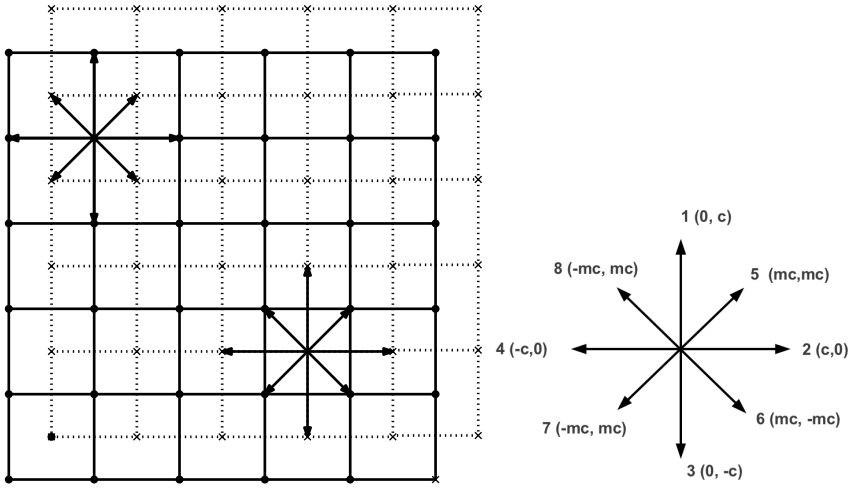

Figure 2.8: As shown in left figure we have a replica structure introduced by a space translation of original lattice by amount $(\Delta x/2, \Delta y/2)$.Figure on right shows composite lattice created by such replica structure. Here the stencil set is union of two energy shells with the magnitude in the energy shell in the ratio of $1\colon 2m^2$ with $m = 1/2$

will map on itself via space translation of $(\Delta x, 0), (0, \Delta x)$. In current replica structure, we have introduced translation invariance with respect to $(\Delta x/2, \Delta x/2)$ also. In this case of replica lattice, the stencil set is union of two energy shells with the magnitude in the energy shell in the ratio of $1\colon 2m^2$ with $m = 1/2$. Using Eq.2.33, we can search for weights and unit cell spacing c for such arbitrary displaced lattice parameterized in term of displacement m. Notice that $m = 1/2$ correspond to present case, while $m = 1$ represent standard D2Q9 model used in LB. For such a set Eq.2.33 simplifies as:

$$\begin{aligned} w_0 + 4\,w_1 + 4\,w_2 &= 1, \\ 2w_1 + 4m^2 w_2 &= \frac{\epsilon}{c^2}, \\ 2w_1 + 4w_2 m^4 &= \frac{3\,\epsilon^2}{c^4}, \\ 4w_2 m^4 &= \frac{\epsilon^2}{c^4}, \end{aligned} \tag{2.36}$$

which can be inverted to obtain the weights and ϵ for this stencil as:

$$w_0 = \frac{4\epsilon^2}{c^4 m^2}, \quad w_1 = \frac{\epsilon^2}{c^4}, \quad w_2 = \frac{\epsilon^2}{4c^4 m^4}, \quad \epsilon = \frac{c^2 m^2}{2m^2 + 1}. \tag{2.37}$$

If $m = 1$ in the Eq. 2.37, the weights correspond to the standard D2Q9 model and the weights corresponding to $m = \frac{1}{2}$ in Eq. 2.37 are named as the replica D2Q9 weights.

In Table. 2.2, $m = 1$, represents the weights for the standard D2Q9 model, and $m = 1/2$, represents weights for the replica D2Q9 model. These models ensure isotropy upto fourth order. Later, we shall show that replica structure is superior for numerical implementations.

2.5 Operator Formulation *via* Generating Function

The discrete generator contains all the information about discrete version of differential operators. In this section, we show that any desired discrete operator can be formed by taking appropriate derivative of the generating function given by the Eq. 2.22. As for example, the discrete gradient operator acting on a scalar field $\psi(\mathbf{r})$ can be obtained via relation:

$$\widetilde{\boldsymbol{\nabla}}\left[\psi(\mathbf{r})\right] = \frac{1}{\epsilon}\frac{d\tilde{G}}{ds_i}\left[\psi(\mathbf{r})\right] \equiv \frac{1}{\epsilon}\sum_i w_i \mathbf{e}_i \psi(\mathbf{r}+\mathbf{e}_i), \tag{2.38}$$

which upon Taylor-series expansion, on the set of stencils with above mention desired properties of closure the, yields

$$\widetilde{\boldsymbol{\nabla}}\psi(\mathbf{r}) = (1+\frac{\epsilon}{2}\nabla^2)\nabla\psi(\mathbf{r}) + \cdots, \tag{2.39}$$

From this expression, we can see that the gradient operator is recovered with isotropic error of $O(\epsilon)$ (Ramadugu *et al.* 2013). Similarly, we can show that(Ramadugu *et al.* 2013)

$$\widetilde{\nabla}_\alpha F_\alpha = \frac{1}{\epsilon}\frac{d\tilde{G}}{ds_\alpha}F_\alpha(\mathbf{r}) = \frac{1}{\epsilon}\sum_i w_i e_{i\alpha} F_\alpha(\mathbf{r}+\mathbf{e}_i), \tag{2.40}$$

which approximates the continuous operator with an error of $O(\epsilon)$ as

$$\widetilde{\nabla}_\alpha F_\alpha = \left(1+\frac{\epsilon}{2}\nabla^2\right)\nabla_\alpha F_\alpha. \tag{2.41}$$

Similarly, the discrete curl operator on vector field $\boldsymbol{\phi}(\mathbf{r})$ defined on the grid is:

$$\widetilde{\boldsymbol{\nabla}}\times\boldsymbol{\phi} = \frac{1}{\epsilon}\frac{d\tilde{G}}{d\mathbf{s}}\times\boldsymbol{\phi}(\mathbf{r}) = \frac{1}{\epsilon}\sum_{i=1}^{N} w_i \mathbf{e}_i \times \boldsymbol{\phi}(\mathbf{r}+\mathbf{e}_i), \tag{2.42}$$

which approximates the continuous operator with an error of $O(\epsilon)$ as

$$\widetilde{\boldsymbol{\nabla}}\times\boldsymbol{\phi} = \left(1+\frac{\epsilon}{2}\nabla^2\right)\boldsymbol{\nabla}\times\boldsymbol{\phi}. \tag{2.43}$$

Finally, from the basic definition of the operator (Eq.2.21), it is evident that the generator can be used to obtain discrete laplacian as

$$\widetilde{\nabla}^2\psi(\mathbf{r}) = \frac{2}{\epsilon}\sum_i w_i\left[\psi(\mathbf{r}+\mathbf{e}_i)-\psi(\mathbf{r})\right], \tag{2.44}$$

Using Eq.2.21,we see that

$$\widetilde{\nabla}^2\psi(\mathbf{r}) = \left(1+\frac{\epsilon}{4}\nabla^2\right)\nabla^2\psi(\mathbf{r}). \tag{2.45}$$

which is an $O(\epsilon)$ representation for laplacian (Ramadugu *et al.* 2013; Thampi *et al.* 2012).

2.6 Higher Order Operators

In the previous section, we saw that in the present formalism, that for every continuous operator $\mathcal{F}$, the equivalent discrete counterpart $\tilde{\mathcal{F}}$ in an $O(\epsilon)$ representation is of the form

$$\tilde{\mathcal{F}} = \left(1 + \frac{a\epsilon}{2}\nabla^2\right)\mathcal{F}, \tag{2.46}$$

where a is a constant and $a = 1$ for gradient, curl and divergence, $a = 1/2$ for laplacian. Following (Lele 1992), this expression can be written as

$$\tilde{\mathcal{F}} = \left(1 + \frac{a\epsilon}{2}\tilde{\nabla}^2\right)\mathcal{F}, \tag{2.47}$$

where laplacian is replaced with its discrete representation with $O(\epsilon)$ validity. At this point, we have a compact matrix representation for the discrete operator and one could use methodology developed in (Lele 1992) to obtained $O(\epsilon^2)$ representation of the operator. It should be noted that unlike standard finite difference an isotropic operator has lead to error term, which can be conveniently inverted almost similar to one dimensional case.

In this thesis, we follow an alternate procedure, where we perform analytical inversion to obtain $O(\epsilon^2)$ accurate representation as

$$\hat{\mathcal{F}} = \left(1 - \frac{a\epsilon}{2}\tilde{\nabla}^2\right)\hat{\mathcal{F}}. \tag{2.48}$$

Thus, we have a simple procedue where first second order accurate representation is obtained and then refinement is done via Eq.2.48. This procedure can be thought as optimal generalization of compact scheme of (Lele 1992). It should be noted that on the isotropic lattices discussed in the thesis, fourth order operator will not remain isotropic. If we wish to obtain isotropy for fourth order operator, the discrete generator should be exact for a sixth order polynomials.

2.7 Results

In this section, we shall evaluate the effectiveness of the present isotropic operator and replica grid. Firstly, the isotropy of the operator is verified by taking the discrete fourier transform(DFT) of any operator $\mathcal{F}$ defined as

$$\mathcal{F}(\mathbf{k}) = \frac{\sum_r \exp(-i\mathbf{k}\cdot\mathbf{r})\mathcal{F}[\psi]}{\sum_r \exp(-i\mathbf{k}\cdot\mathbf{r})\psi(\mathbf{r})}. \tag{2.49}$$

The DFT of the discrete laplacian can be computed via Eq. 2.46 for the lattice based schemes as:

$$\tilde{\nabla}^2(\mathbf{k}) = -k^2\left(1 - \frac{\epsilon}{4}k^2\right). \tag{2.50}$$

In Table: 2.3, discrete laplacian is reported for the standard and replica D2Q9 lattice along with equivalent expression for central difference operator. It is evident that while D2Q9 model results in isotropic laplacian, amplitude of the error is more than central difference operator. We can also see that on the replica lattice both amplitude and phase error are smaller than CD2 operator.

Similarly, for fourth order laplacians based on standard D2Q9 weights(L4) and replica D2Q9 weights (RL4) schemes fourier transforms are also calculated similarly and the same are plotted on a polar plot in Fig.2.9. In the plot, the radius is normalized by exact value of the laplacian (i.e),$-k^2$. It is evident that the same qualitative behaviour exist for fourth order operators too and replica lattice is superior in all the cases.

In Table2.4, the DFT of the 3D laplacian for both the standard models and replica model is calculated and contrasted with existing result in the literature. It is evident that replica scheme is more efficient both in terms of the phase error as well as amplitude error. Furthermore, this isotropy is achieved with just 15-point stencil, unlike 27 value mentioned in the literature.

2.7.1 Fourier Analysis for Gradient Operator

A similar analysis for the gradient operator shows that

$$D(\mathbf{k})_\alpha = ik_\alpha \left(1 - \frac{\epsilon}{2}k^2 + \frac{\epsilon^2}{8}k^4 + O(k^6)\right), \tag{2.51}$$

which show that the lattice based gradient operators are isotropic. In the small wavelength limit, the corresponding expressions for different fourth order gradient using standard DnQm models and the standard second order central difference ($CD2$) scheme may be written as follows. For clarity, only one component is shown below.

$$D(\mathbf{k})_\alpha^{DnQm} = ik_\alpha \left[1 - \left(\frac{k^4}{36} + \frac{k_\alpha^4}{180} + a\frac{k_\beta^2 k_\gamma^2}{36}\right) + O(k^6)\right] \tag{2.52}$$

$$D(\mathbf{k})_\alpha^{CD2} = ik_\alpha \left[1 - \frac{k_\alpha^2}{6} + O(k^4)\right] \tag{2.53}$$

where $k = |\mathbf{k}|$ and $(\alpha \neq \beta \neq \gamma)$ are the cartesian indices and $a = 0$ for D2Q9 and D3Q27 models, $a = 1$ for D3Q19 and $a = 2$ for D3Q15. It is evident from the Eq. 2.53, that the central difference operator is anisotropic even at the second order and from Eq. 2.52, it is evident that all DnQm models are isotropic at second order but anisotropic at fourth order but, the anisotropy is very less.

2.7.2 Discrete Operators: Green's Function For 2-D Laplacian

As a first example, we shall consider the action of discrete laplacian on $f(x, y) = (log|r|)/(2\,\pi)$, the green function for the 2-D laplace equation. In order to show the effectiveness of the current approach, we calculate the discrete laplacian using isotropic laplacian operator on D2Q9 lattice. The discrete laplacian accurate upto $O(\epsilon)$ is:

$$\tilde{\nabla}^2 f = \frac{8c^2}{r^4}. \tag{2.54}$$

It is evident from this expression and Eq.2.8 that though the error in discrete laplacian obtained from D2Q9 lattice is isotropic, the absolute magnitude of the error has increased in lattice formulation. On the other hand, if we use replica stencil the discrete laplacian of the 2-D

values,	$m = \frac{1}{2}$	$m = 1$
w_0	$4/9$	$4/9$
w_1	$1/36$	$1/9$
w_5	$1/9$	$1/36$
ϵ	$c^2/6$	$c^2/3$

Table 2.2: Weights and ϵ values for different values of m.

Scheme	$\tilde{\nabla}^2(\mathbf{k})$	stencil size
CD2	$\tilde{\nabla}^2(\mathbf{k}) = -k^2(1 - \frac{k^2}{12}(1 - \frac{\sin^2(2\theta)}{2}) + O(k^4))$	5
L2	$\tilde{\nabla}^2(\mathbf{k}) = -k^2(1 - \frac{k^2}{12} + O(k^4))$	9
RL2	$\tilde{\nabla}^2(\mathbf{k}) = -k^2(1 - \frac{k^2}{24} + O(k^4))$	9

Table 2.3: Comparision of different 2D Laplacian operator in fourier mode $\mathcal{L}(\mathbf{k})$ in low wave number limit with the other standard Central difference operator.

Scheme	$\mathcal{L}(\mathbf{k})$	stencil size
(Thampi *et al.* 2012)($L2_{D3Q15}$)	$\mathcal{L}(\mathbf{k}) = -k^2\left(1 - \frac{k^2}{12}\right) + O(k^6)$	15
$RL2_{D3Q15}$	$\mathcal{L}(\mathbf{k}) = -k^2\left(1 - \frac{k^2}{24}\right) + O(k^6)$	15
(Kumar 2004)	$\mathcal{L}(\mathbf{k}) = -k^2\left(1 - \frac{k^2}{12}\right) + O(k^6$	27
(Patra & Karttunen 2006)	$\mathcal{L}(\mathbf{k}) = -k^2\left(1 - \frac{k^2}{12}\right) + O(k^6$	27

Table 2.4: Comparision of stencil sizes of different 3D Laplacian operator in fourier mode $\mathcal{L}(\mathbf{k})$ in low wave number limit with the other standard models.

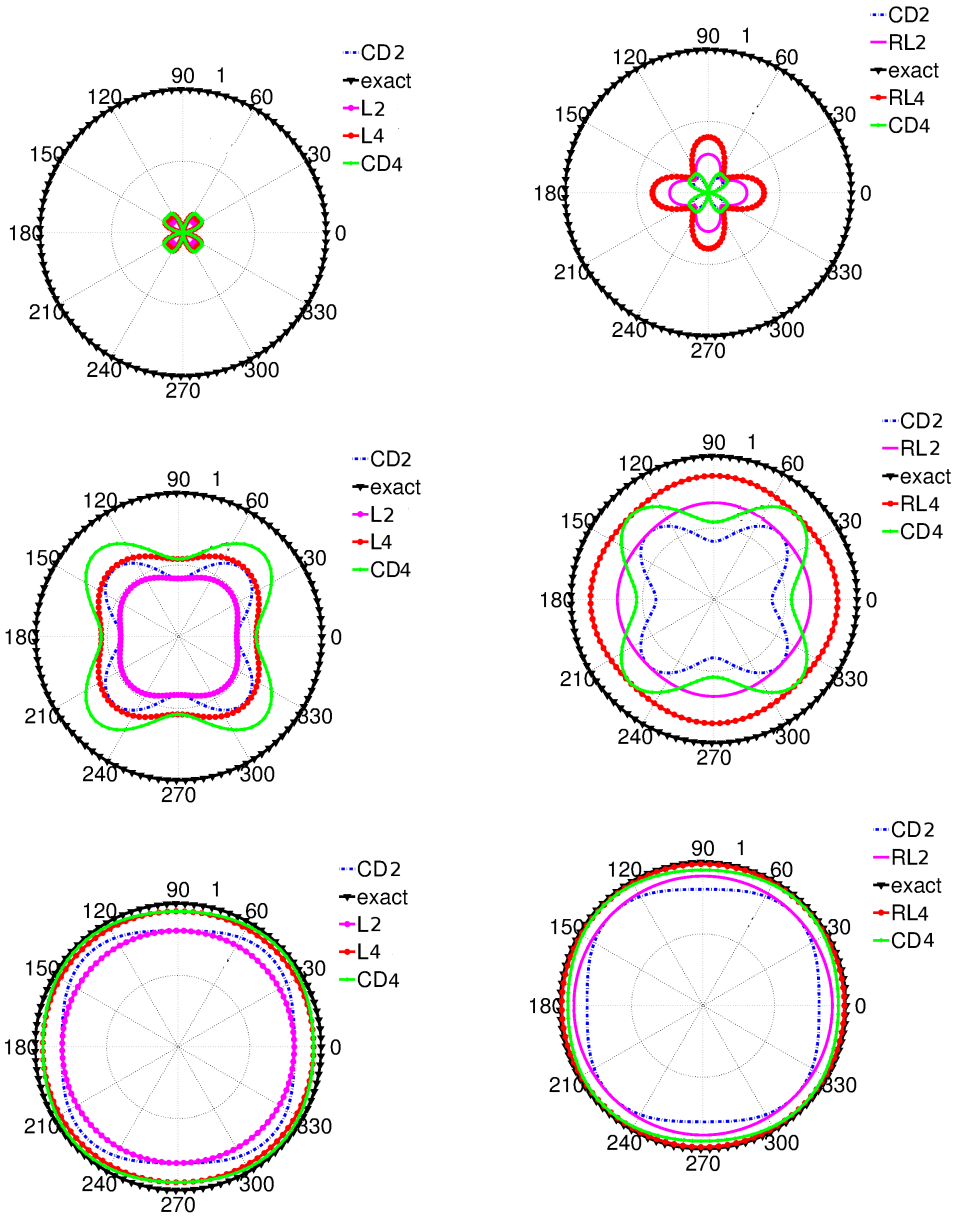

Figure 2.9: Comparision of DFTs of different 2D laplacian operators on polar plot. These plots are plotted for varying the number of points per wave length as 2 (Top), 4 (Middle) and 8 (Bottom). Here L2 represents the lattice laplacian of second order , L4 represents the lattice laplacian of fourth order, CD2 represents the second order central difference, CD 4 represents fourth order central difference, RL2 represents replica lattice laplacian of second order and RL4 represents replica lattice laplacian of fourth order.

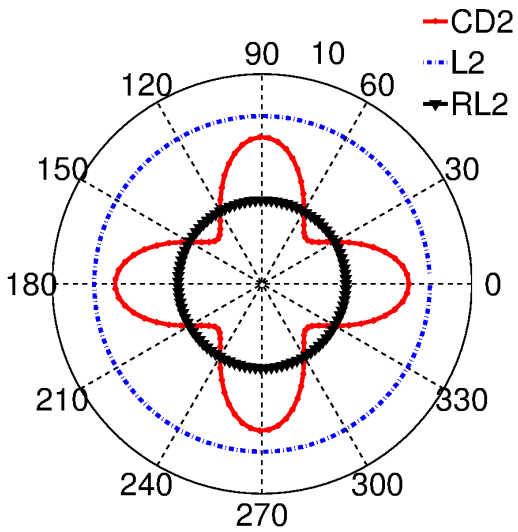

Figure 2.10: Polar plot of the laplacian of Green's function for all the second order schemes shown in Table. 2.5. Here the radius of the plot represents the normalized error.

scheme	laplacian of Green's function
CD2	$\tilde{\nabla}^2 = \frac{c^2}{r^4}\left(7 - 16\cos^2\theta\sin^2\theta\right)$
L2	$\tilde{\nabla}^2 f = \frac{8c^2}{r^4}$
RL2	$\tilde{\nabla}^2 f = \frac{4c^2}{r^4}$

Table 2.5: Comparision of laplacian of 2D Gaussian using replica D2Q9 lattice laplacian(RL2) operators and the lattice D2Q9 laplacian operator(L2)(Thampi *et al.* 2012) with the central difference laplacian operator

.

Green's function accurate upto $O(\epsilon)$ is:

$$\tilde{\nabla}^2 f = \frac{4c^2}{r^4}, \tag{2.55}$$

thus, we see that unlike standard D2Q9 lattice, current formulation leads to lower error in both amplitude as well as phase. The discrete laplacian of the Green's function is summarized in Table 2.5, where we see that replica lattice is most efficient.

This property is more evident in Fig. 2.10, where polar plot (normalized by r^4/c^2) of the discrete laplacian of Green's function for all the second order schemes is shown. We remind that ideally laplacian of the chosen function should be zero, thus for any given scheme ideally we would like the shape to be circular and radius of the circle to be as small as possible.

Chapter 3

Isotropic Discretization of Linear Partial Differential Equations

3.1 Introduction

A discrete isotropic operators were formulated from a generating function in the previous chapter. Furthermore, a concept of replica grid was introduced where discrete operator with second as well as fourth order accuracy were developed. In this chapter, we shall apply these operators to a host of partial differential equations and investigate the efficiency of this new approach. In particular, examples of linear advection equation, diffusion equation and wave equation is considered. Such PDE's have application in various fields such as fluid mechanics, classical electrodynamics, wave dynamics etc.

We know that even when PDE's are non dispersive,the discrete model of the same will be dispersive (Trefethen 1996, 1982) (i.e) the numerical solutions creates spurious dispersion and because of which the shape of the initial function will not be preserved. Group velocity and phase velocity are to be studied in order to understand such behavior of the numerical schemes (Vichnevetsky & Bowles 1982). In this chapter, we shall discuss about the discretization of PDEs along with the dispersion and thereby the group velocity and phase velocity of the discrete models.

The organisation of the chapter is as follows: In Sec. 3.2, dispresion relation and the group and phase velocities of the semi-discretized advection, wave and diffusion equation is discussed. In Sec. 3.3, isotropic MacCormack method for solving the advection equation is discussed. In Sec. 3.4, the discretization of the diffusion equation by using CD2, RL2 schemes is discussed. In Sec. 3.5, the discretization of wave equation using CD2, RL2 and RL4 is discussed. The dispersion relations and the group and phase velocities of the same are also discussed in the same section. Sec. 3.6 discusses the discretization of Maxwell equations using Yee scheme, RL2 and RL4 methods along with the dispersion relations.

3.2 Dispersion Relation for Semi-Discrete Approximations

PDEs with constant coeffcients on an unbounded space domain admits plane wave solutions of the form

$$u(\mathbf{x}, t) = \hat{u} \exp\left(I\left(k_i x_i + \omega t\right)\right), \tag{3.1}$$

where $\hat{u}$ is constant amplitude, $\boldsymbol{k}$ is the wave number and ω is the frequency. For each value of vector $\boldsymbol{k}$, PDE imposes a relationship between wavenumber and frequency

$$\omega = \omega\left(\boldsymbol{k}\right), \tag{3.2}$$

known as dispersion relationship. In general, for nth order (in time) PDE each wavenumber $\boldsymbol{k}$ correspond to n different frequency. For real wavenumber $\boldsymbol{k}$, the wave decays with time if $\mathrm{Im}\,\omega > 0$ and decays if $\mathrm{Im}\,\omega < 0$. For the propogating wave, the phase velocity is defined as the rate at which the phase of the wave propagates in space and is given by:

$$c^{\text{phase}} = \frac{\omega}{k}. \tag{3.3}$$

However, it is often more informative to introduce group velocity, which is defined as the velocity with which the envelop of wave propagates through the space (Brillouinn 1960) and is given by:

$$c^{\text{group}} = \frac{\partial \omega}{\partial k}, \tag{3.4}$$

where ω is the angular velocity of the wave and k is the angular wave number. Though, it is desirable that when the PDE is discretized, the group and phase velocities should have minimum possible error, in practice often group velocity at high wave number shows unphysical oscillations.

The dispersion relation for some of important model equations and their semi-discrete approximations, where spatial derivatives are replaced by second order spatial approximation, are:

- **Advection Equation:** For the advection equation with velocity v_i

  $$u_t + v_i \partial_i u = 0, \tag{3.5}$$

  dispersion relation is

  $$\omega = -v_i k_i, \tag{3.6}$$

  which implies that both group and phase velocity is propagation velocity v_i. If we replace space derivative by central difference we have dispersion relation as

  $$\omega^{\text{CD2}} = -\frac{1}{c}\sum_{i=1}^{D} v_i \sin\left(k_i\, c\right), \tag{3.7}$$

  where c is the grid spacing. On the other hand, the dispersion relation for the advection equation in 2D using the replica D2Q9 weights is:

  $$\omega^{\text{RL2}} = -\frac{1}{3c}\left[v_x\left\{\sin\left(k_x\, c\right) + 4\sin\left(\frac{k_x\, c}{2}\right)\cos\left(\frac{k_y\, c}{2}\right)\right\} + v_y\left\{\sin\left(k_y\, c\right) + 4\sin\left(\frac{k_y\, c}{2}\right)\cos\left(\frac{k_x\, c}{2}\right)\right\}\right]. \tag{3.8}$$

  The dispersion relation using RL4 scheme is:

  $$\omega^{\text{RL4}} = \left[1 + \frac{1}{36}\left\{10 - \cos(k_x c) - \cos(k_y c) - 8\cos\left(\frac{k_x c}{2}\right)\right\}\right]\omega^{\text{RL2}}. \tag{3.9}$$

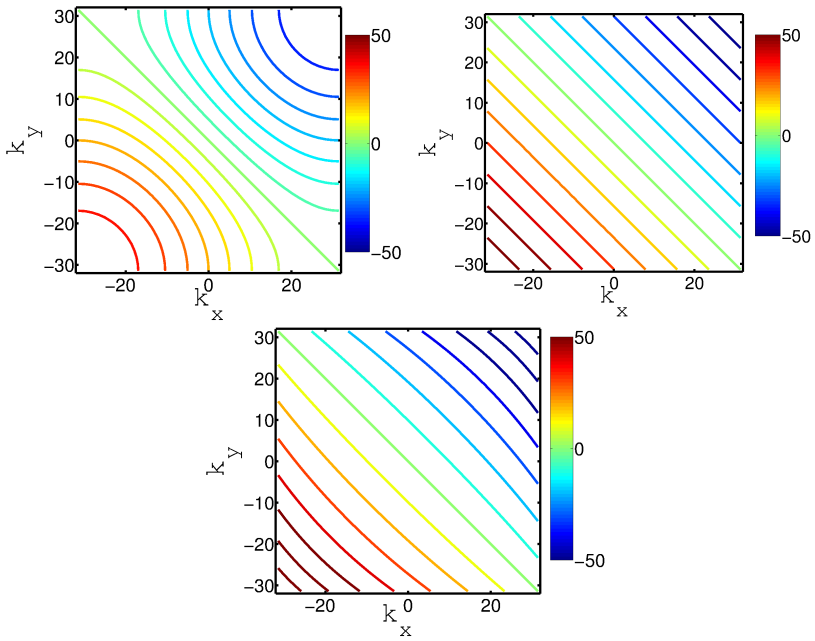

Figure 3.1: Isocontours of dispersion relation for advection equation for CD2(Top left),exact(Top right) and RL2 operator (Bottom).

Dispersion relation for advection equation for continuous and second order discrete approximations are contrasted in Fig. 3.1 for 2D case. This plot shows that while at low wave number dispersion relation obtained from CD operator is indeed a good approximate representation of the continuous one.Fig. 3.2 shows that the RL2 and RL4 operator has improved accuarcy compared to the CD2 operator.RL4 operator has the best accuarcy of all.R

In discrete case, group velocity is

$$c_j^{\text{group, CD2}} = -v_j \, \frac{kj}{k} \cos\left(k_j \, c\right), \tag{3.10}$$

while phase velocity is

$$c_j^{\text{phase, CD2}} = -\frac{1}{k_j \, c} \sum_{i=1}^{D} v_i \sin\left(k_i \, c\right), \tag{3.11}$$

Notice that while phase and group velocity are same at very low wavenumber, their behaviour is quite different from each other as well as from exact relation. If the group velocity and phase velocity of the discretized equation is not same as the exact one the wave propagates with a different speeds which changes the original characteristics of the wave(Trefethen 1982, 1996). The group and phase velocities for the semi discrete advection

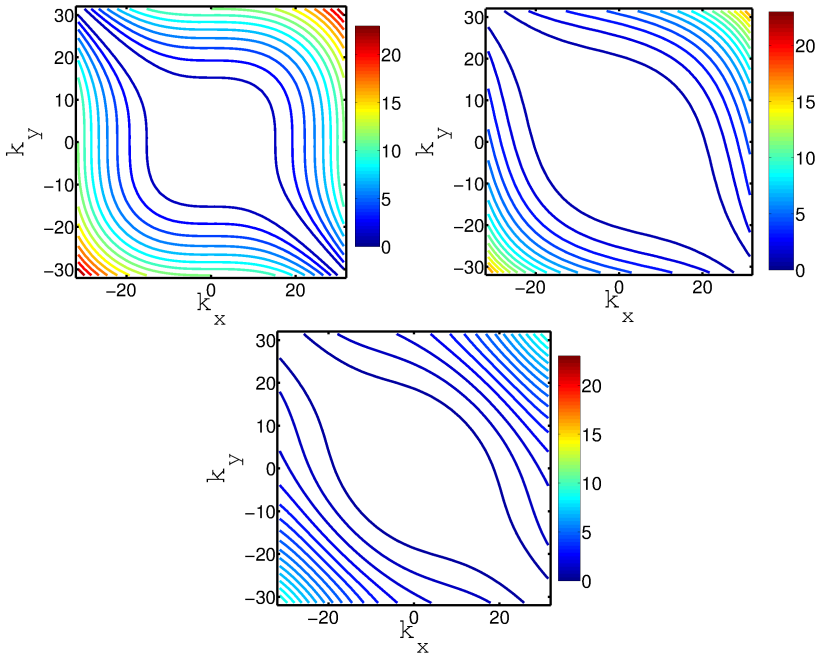

Figure 3.2: Isocontours of error in dispersion relation for advection equation for CD2(Top left), RL2(Top right) and RL4 operator (Bottom) w.r.t the exact dispersion relation.

equation using RL2 operator are

$$
\begin{aligned}
c^{\text{group, RL2}} &= -\frac{1}{3ck}\left[v_x k_x \left\{\cos\left(k_x\, c\right) + 2k_x \cos\left(\frac{k_x c}{2}\right)\cos\left(\frac{k_y\, c}{2}\right) - 2k_y \sin\left(\frac{k_x c}{2}\right)\sin\left(\frac{k_y c}{2}\right)\right\}\right. \\
&\quad \left. + v_y k_y \left\{\cos\left(k_y\, c\right) + 2k_y \cos\left(\frac{k_y\, c}{2}\right)\cos\left(\frac{k_x\, c}{2}\right) - 2k_x \sin\left(\frac{k_y\, c}{2}\right)\sin\left(\frac{k_x\, c}{2}\right)\right\}\right] \\
c^{\text{phase, RL2}} &= -\frac{1}{3ck}\left[v_x \left\{\sin\left(k_x\, c\right) + 4\sin\left(\frac{k_x\, c}{2}\right)\cos\left(\frac{k_y\, c}{2}\right)\right\} + v_y \left\{\sin\left(k_y\, c\right) + 4\sin\left(\frac{k_y\, c}{2}\right)\cos\left(\frac{k_x\, c}{2}\right)\right\}\right.
\end{aligned}
\tag{3.12}
$$

The normalized group and phase velocities for semi discretized advection equation using CD2 and RL2 operators are reported in Fig. 3.3 and Fig. 3.4 respectively. The group

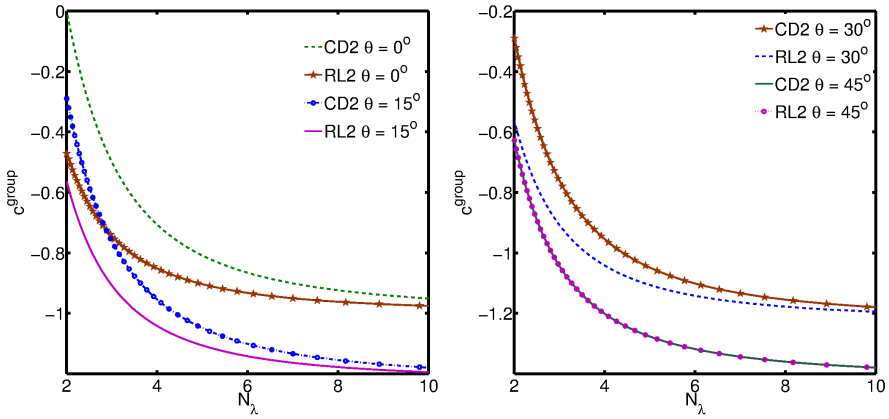

Figure 3.3: The normalized group velocity for semi discretized advection equation using CD2 and RL2 operator for different propagation angles.

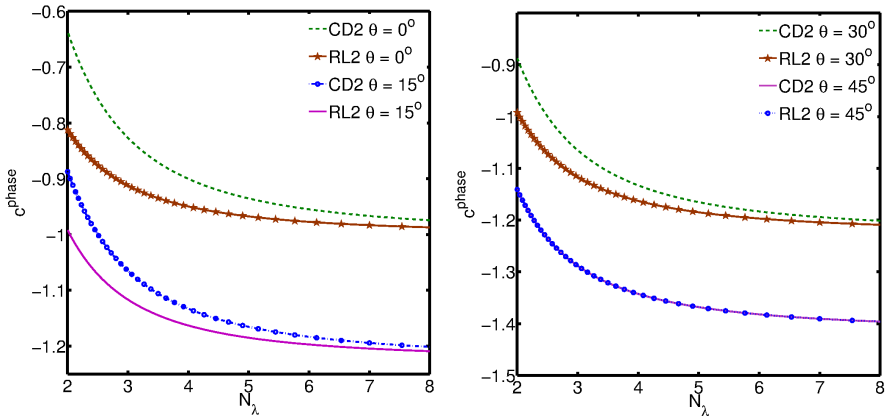

Figure 3.4: The normalized phase velocity for semi discretized advection equation using CD2 and RL2 operator for different propagation angles.

and phase velocities are dependent on the angle of propagation for CD2 operator but in the case of the RL2 operator, the group and phase velocities are independent of angle of propagation.

- **Wave Equation:** For the wave equation with wave speed c_s

$$u_{tt} = c_s^2 \nabla^2 u, \tag{3.13}$$

dispersion relation is

$$\omega^2 = c_s^2 k^2. \tag{3.14}$$

If we replace space derivative by central difference we have dispersion relation as

$$\left(\omega^{\mathrm{CD2}}\right)^2 = \frac{4D}{c^2} \sum_{i=1}^{D} \sin^2 \frac{k_i c}{2}, \tag{3.15}$$

Similarly, the dispersion relation using the replica operators is

$$\left(\omega^{\mathrm{RL2}}\right)^2 = \frac{2}{3} \left(\frac{c_s}{c}\right)^2 \left[10 - \cos(k_x c) - \cos(k_y c) - 8 \cos\left(\frac{k_x c}{2}\right) \cos\left(\frac{k_y c}{2}\right)\right]. \tag{3.16}$$

The dispersion relation using RL4 scheme is:

$$\omega^{\mathrm{RL4}} = \left[1 + \frac{1}{36}\left\{10 - \cos(k_x c) - \cos(k_y c) - 8 \cos\left(\frac{k_x c}{2}\right) \cos\left(\frac{k_y c}{2}\right)\right\}\right] \omega^{\mathrm{RL2}}. \tag{3.17}$$

Fig. 3.5 contrasts dispersion relation for 2D wave equation for continuous and second order (in space) discrete approximations. It is evident that the RL2 operator has better accuracy compared to The CD2 operator. The isocontours of error in dispersion relation for 2D wave equation using CD2, RL2 and RL4 operators is shown in Fig. 3.6. It is evident from the figure that RL2 has better accuracy compared to the CD2 operator and RL4 operator has the best accuracy among the three.

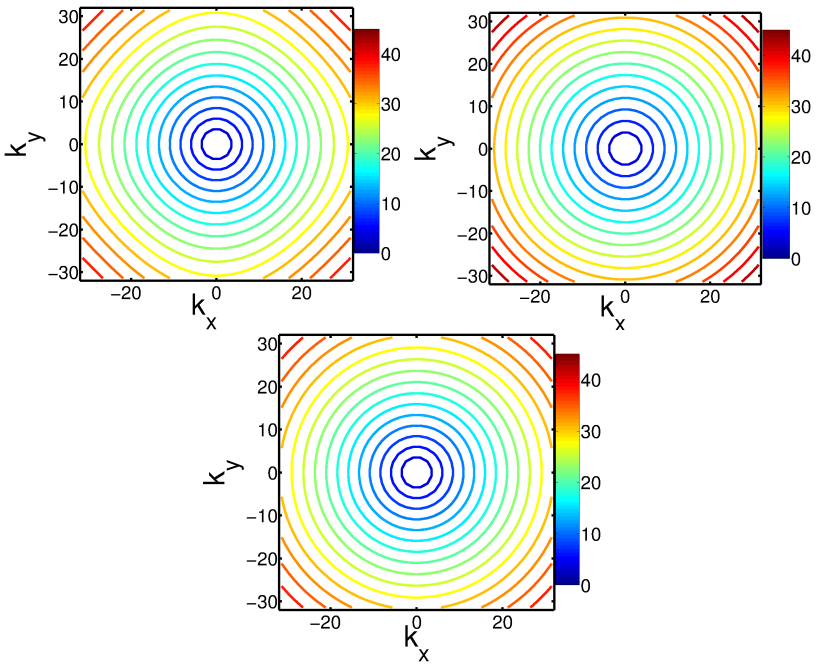

Figure 3.5: Isocontours of dispersion relation for wave equation for CD2(Top left),exact(Top right) and RL2 operator (Bottom).

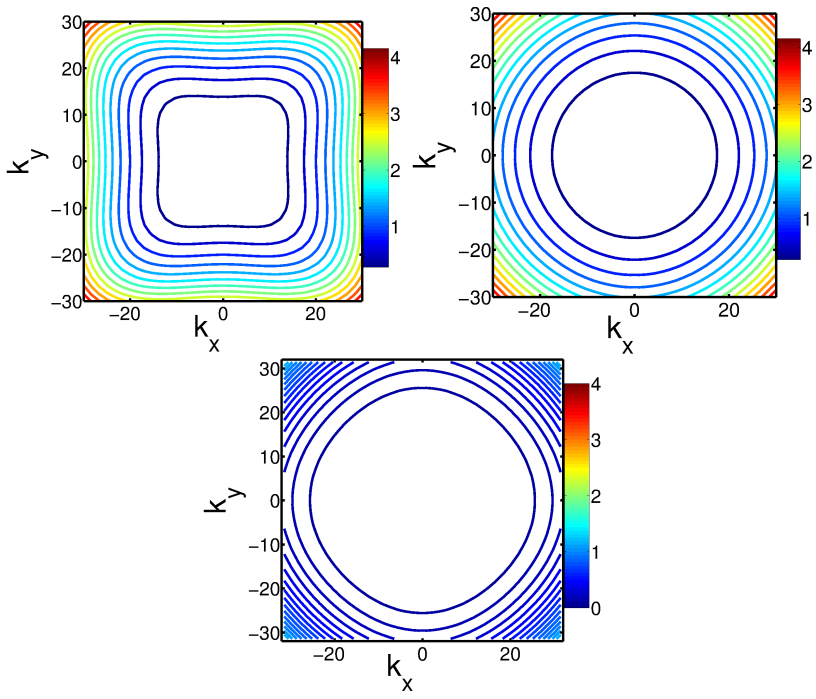

Figure 3.6: Isocontours of error in dispersion relation for wave equation for CD2(Top left), RL2(Top right) and RL4 operator (Bottom) w.r.t the exact dispersion relation.

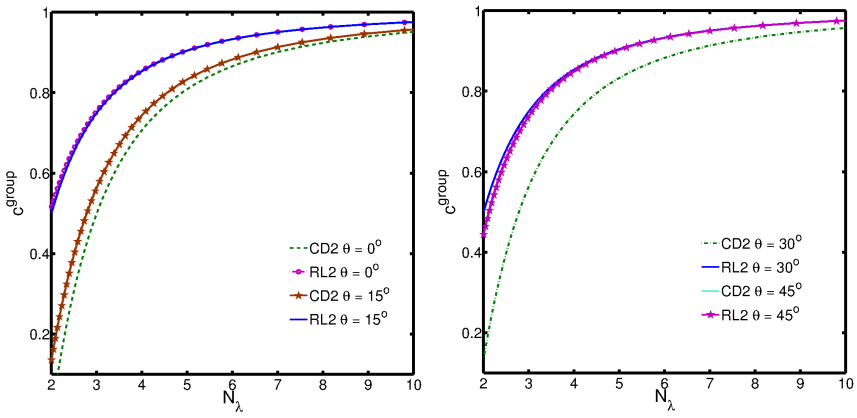

Figure 3.7: The normalized group velocity for semi discretized wave equation using CD2 and RL2 operator for different propagation angles.

The group and phase velocities for the semi discretized wave equation using central difference are as follows:

$$\frac{c^{\text{group, CD2}}}{c_s} = \frac{1}{2k}\frac{\sum_i k_i \sin(k_i c)}{\sqrt{\sum_i \sin^2(k_i c/2)}}, \qquad \frac{c^{\text{phase, CD2}}}{c_s} = \frac{2}{ck}\sqrt{\sum_i \sin^2(k_i c/2)}, \tag{3.18}$$

while the same obtained via RL2 scheme are:

$$\begin{aligned}\frac{c^{\text{group, RL2}}}{c_s} &= \frac{1}{3ck}\left[\sin(k_x c)\frac{k_x}{k} + \sin(k_y c)\frac{k_y}{k} + 4\cos\left(\frac{k_x c}{2}\right)\sin\left(\frac{k_y c}{2}\right)\frac{k_y}{k} + 4\cos\left(\frac{k_y c}{2}\right)\sin\left(\frac{k_x c}{2}\right)\frac{k_x}{k}\right],\\ \frac{c^{\text{phase, RL2}}}{c_s} &= \frac{1}{ck}\sqrt{\frac{2}{3}\left[10 - \cos(k_x c) - \cos(k_y c) - 8\cos\left(\frac{k_x c}{2}\right)\cos\left(\frac{k_y c}{2}\right)\right]}.\end{aligned} \tag{3.19}$$

The phase and group velocities for the semi discretized wave equation using RL2 operator is plotted against the number of points per wave length for different angles of propagation and is reported in Fig. 3.7. It is evident from the figure that for different propagation angles the group and phase velocities are almost same and the error in phase and group velocities has reduced compared to the CD2 operator.

The group and phase velocities normalized with the propagation speed for semi discretized wave equation using CD2 operator is plotted against the number of points per wave length(N_λ) for different angles and the same is reported in Fig. 3.8. We observe that the group and phase velocities are dependent on angle and as N_λ increases the deviation of the phase and group velocities decrease.

- **Diffusion Equation:** For the diffusion equation with diffusivity D

$$u_t = D\,\nabla^2 u, \tag{3.20}$$

dispersion relation is

$$I\,\omega = -D\,k^2, \tag{3.21}$$

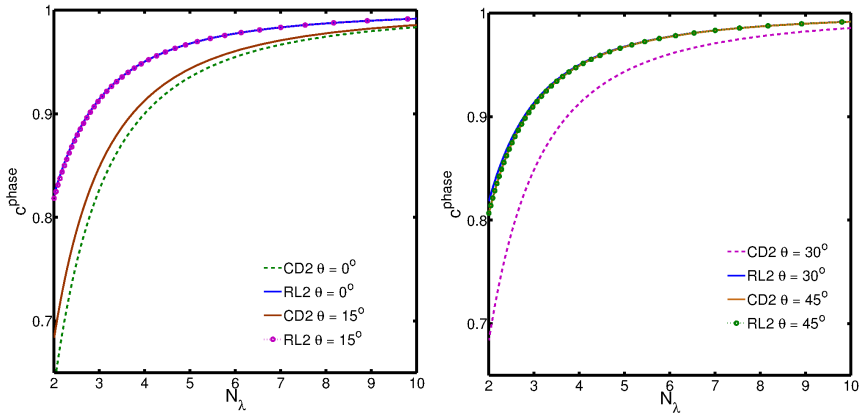

Figure 3.8: The normalized phase velocity for semi discretized wave equation using CD2 and RL2 operator for different propagation angles.

If we replace space derivative by central difference we have dispersion relation as

$$\omega^{\mathrm{CD2}} = -\frac{4\,c_s^2}{c^2}\sum_{i=1}^{D}\sin^2\frac{k_i\,c}{2}, \tag{3.22}$$

while the same obtained from RL2 scheme is:

$$\omega^{\mathrm{RL2}} = -\frac{4\,c_s^2}{c^2}\frac{2}{3}\left[10-\cos(k_x c)-\cos(k_y c)-8\cos\left(\frac{k_x c}{2}\right)\cos\left(\frac{k_y c}{2}\right)\right]. \tag{3.23}$$

The dispersion relation using RL4 scheme is:

$$\omega^{\mathrm{RL4}} = \left[1+\frac{1}{36}\left\{10-\cos(k_x c)-\cos(k_y c)-8\cos\left(\frac{k_x c}{2}\right)\cos\left(\frac{k_y c}{2}\right)\right\}\right]\omega^{\mathrm{RL2}}. \tag{3.24}$$

Dispersion relation for 2D diffusion equation for continuous and with CD2 and RL2 operator is reported in Fig. 3.9. It is evident from figure that the CD2 operator is not isotropic and at high wave numbers the magnitude of error is high for CD2 operator.Isocontours of error in dispersion relation w.r.t continuous for CD2, RL2 and RL4 operators is reported in Fig. 3.10. It is evident from the figure that RL2 and RL4 have better accuracy and isotropy compared to the CD2 operator.

From the dispersion relation for representative linear PDE's, it is evident that in all cases, the dispersion relation in discrete case is a faithful representation of continuous one provided wavenumber is very close to zero. There are previous studies on discretization of Eq. 3.13 using the dispersion relation preserving schemes(Tam & Webb 1993; Tam & Kurbatskii 2003; Cheong & Lee 2001).

As discussed in previous chapter, these schemes are not isotropic because they are restrained to the principal directions only. In the subsequent section, we shall discuss the dispersion relation and thereby group and phase velocities with the isotropic operators.

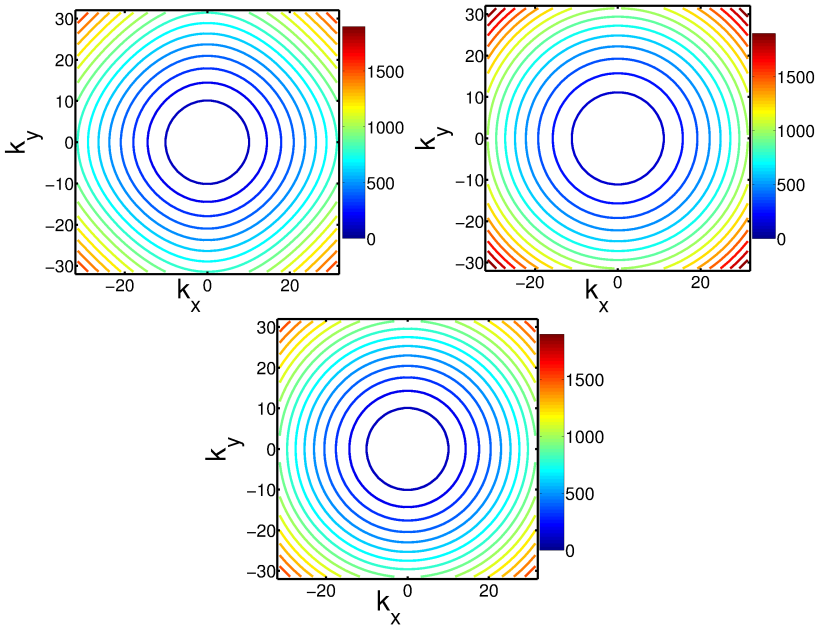

Figure 3.9: Isocontours of dispersion relation for diffusion equation for CD2(left), exact(centre) and RL2 operator (right).

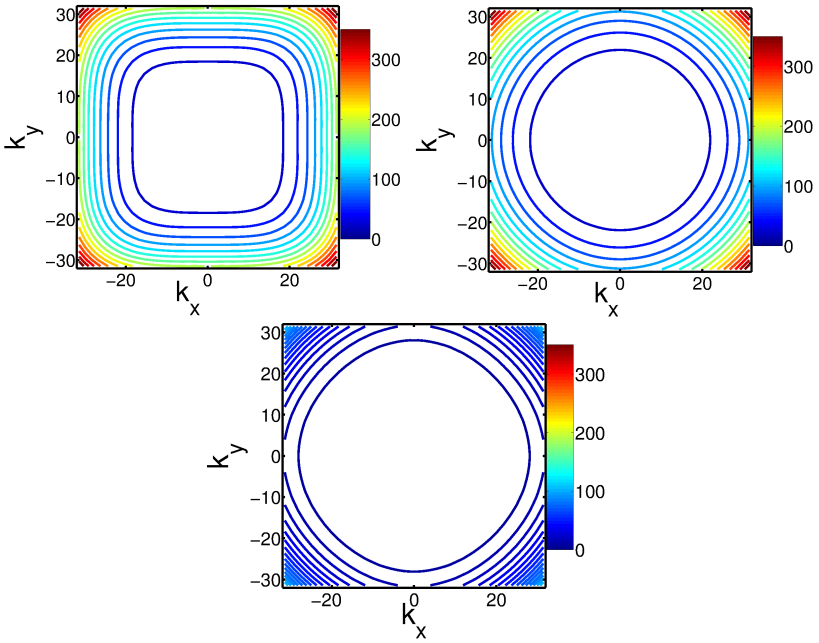

Figure 3.10: Isocontours of error in dispersion relation for diffusion equation for CD2(left), RL2(centre) and RL4 operator (right) w.r.t the continuous dispersion relation.

3.3 Discrete Time Stepper for Advection Equation

In last section, it was showen that current isotropic formulation of the derivatives are superior at least in the semi discrete sense. In this section, we show that after appropriate time discretization the present isotropic approach leads to far superior results over conventional approaches. As a first example, we employ cuurent approach for the advection equation. For the advection equation, we chose as time integrator MacCormack method, an elegant method for discretizing the advection equation(Laney 1998; LeVeque 2007) The method is widely used due to its simplicity and robustness for the non-linear case (see for example (Selle *et al.* 2008)). In this method, a two step integration procedure is adopted, where in the predictor step first order forward Euler is used for time discretization and in space also a first order scheme (either forward or backward) is used. In the corrector step, backward Euler is used for time discretization and space derivative is first order but opposite to the forward step. In order to keep the method explicit, in corrector step the spatial derivative are evaluated with the predicted value. Finally, one averages the two solutions to get a second order accurate representation. In particular, the method in 2-D can be formulated as follows:

- **Predictor Step**

$$u^{\star}_{i,j} = u^{n}_{i,j} - v_x \frac{\Delta t}{\Delta x}\left(u^{n}_{i+1,j} - u^{n}_{i,j}\right) - v_y \frac{\Delta t}{\Delta y}\left(u^{n}_{i,j+1} - u^{n}_{i,j}\right), \tag{3.25}$$

  Where $u^{n}_{i,j}$ is the value of u at (i,j) point in space and n is the time level and $u^{\star}_{i,j}$ is the predicted value of u at (i,j) point in space.

- **Corrector Step**

$$u^{\star\star}_{i,j} = u_{i,j} - v_x \frac{\Delta t}{\Delta x}\left(u^{\star}_{i,j} - u^{\star}_{i-1,j}\right) - v_y \frac{\Delta t}{\Delta y}\left(u^{\star}_{i,j} - u^{\star}_{i,j-1}\right), \tag{3.26}$$

  finally, the solution at $n+1$ time can be reconstructed as

$$u^{n+1}_{i,j} = \frac{1}{2}\left(u^{\star}_{i,j} + u^{\star\star}_{i,j}\right). \tag{3.27}$$

While for linear equations, the MacCormack scheme is equivalent to the LaxâWendroff scheme in case of non-linear advection equation it provides a simple and robust approach to non-linear advection equation. As is the case with usual central schemes, this scheme is also not isotropic.

We wish to apply this approach of time integration with the isotropic operators discussed in the previous chapter. However, the operator discussed in the previous chapters were of central in nature. Thus, we need to create forward and backward decomposition of such operators for applying MacCormack scheme. This can be achived by noting that

$$\tilde{\nabla}_{\alpha}^{\,\mathrm{RL2}} u = \tilde{\nabla}_{\alpha}^{\,\mathrm{RL2+}} u + \tilde{\nabla}_{\alpha}^{\,\mathrm{RL2-}} u, \tag{3.28}$$

where

$$\tilde{\nabla}_{\alpha}^{\text{RL2+}} u = \frac{1}{\epsilon} \sum_{c_{i\beta}\cdot\hat{e}_{\beta}>0} w_i |c_{i\beta}\cdot\hat{e}_{\beta}| \left(u(\mathbf{r}+\mathbf{c}_i) - u(\mathbf{r})\right), \tag{3.29}$$

where $\hat{e}_{\alpha}$ is the unit vector in the α direction. and the backward difference can be expressed as

$$\tilde{\nabla}_{\alpha}^{\text{RL2-}} u = \frac{1}{\epsilon} \sum_{c_{i\beta}\cdot\hat{e}_{\beta}<0} w_i |c_{i\beta}\cdot\hat{e}_{\beta}| \left(u(\mathbf{r}) - u(\mathbf{r}+\mathbf{c}_i)\right), \tag{3.30}$$

Once, this decomposition is done, present isotropic forward and backward operator can be used instead of original forward and backward spatial difference operators. In particular for 2D case, we can write the scheme as follows:

- **Predictor Step**

$$\begin{aligned} u^{\star}_{i,j} = u^{n}_{i,j} &- v_x \frac{\Delta t}{3\Delta x}\left(u^{n}_{i+1,j} + 2u_{i+1/2,j+1/2} + 2u_{i+1/2,j-1/2} - 5u^{n}_{i,j}\right) \\ &- v_y \frac{\Delta t}{\Delta y}\left(u^{n}_{i,j+1} + 2u^{n}_{i+1/2.j+1/2} + 2u_{i-1/2,j+1/2} - 5u^{n}_{i,j}\right), \end{aligned} \tag{3.31}$$

- **Corrector Step**

$$\begin{aligned} u^{\star\star}_{i,j} = u^{n}_{i,j} &- v_x \frac{\Delta t}{3\Delta x}\left(5u^{\star}_{i,j} - 2u^{\star}_{i+1/2,j+1/2} - 2u^{\star}_{i+1/2,j-1/2} + u^{\star}_{i-1,j}\right) \\ &- v_y \frac{\Delta t}{3\Delta y}\left(5u^{\star}_{i,j} - u^{\star}_{i,j-1} - 2u^{\star}_{i+1/2,j+1/2} - 2u^{\star}_{i-1/2,j+1/2}\right), \end{aligned} \tag{3.32}$$

finally, the solution at $n+1$ time can be reconstructed as

$$u^{n+1}_{i,j} = \frac{1}{2}\left(u^{\star}_{i,j} + u^{\star\star}_{i,j}\right). \tag{3.33}$$

As discussed in the previous chapter, we use replica grid with two grids, primary grid and the secondary grid. The secondary grid is displaced by half the grid size in both x and y directions. Unlike staggered grid based method, in present case all variables are defined on both the grids and computations are carried out on both the grids simultaneously.

We considered 2D gaussian function with variance 0.01 as the test case to validate the proposed method. The evolution of gaussian function with time using both standard MacCormack and isotropic MacCormack methods at different times is reported in the Figs. (3.12 - 3.13). The exact solution is shown in Fig. 3.11

It is evident from these figures that the standard MacCormack method is not isotropic whereas the modifed MacCormack method is isotropic as well as more accurate and is as simple to implement as the standard MacCormack method. This can also be seen from the L^2-norm is calculated for standard MacCormack and isotropic MacCormack method at time$=1$ and the same is shown in Fig. 3.14.

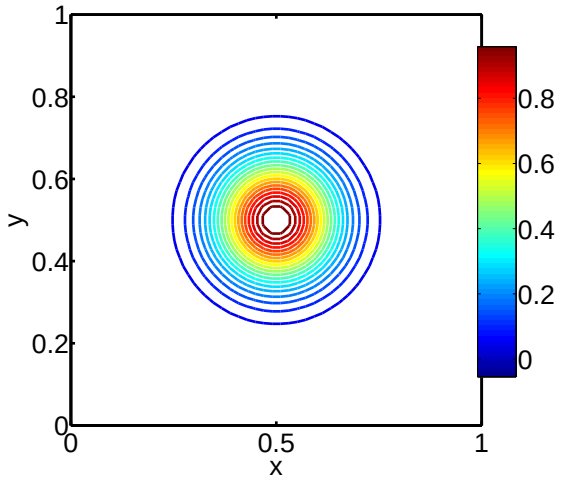

Figure 3.11: Analytical solution of the 2D Gaussian function at time = 1.

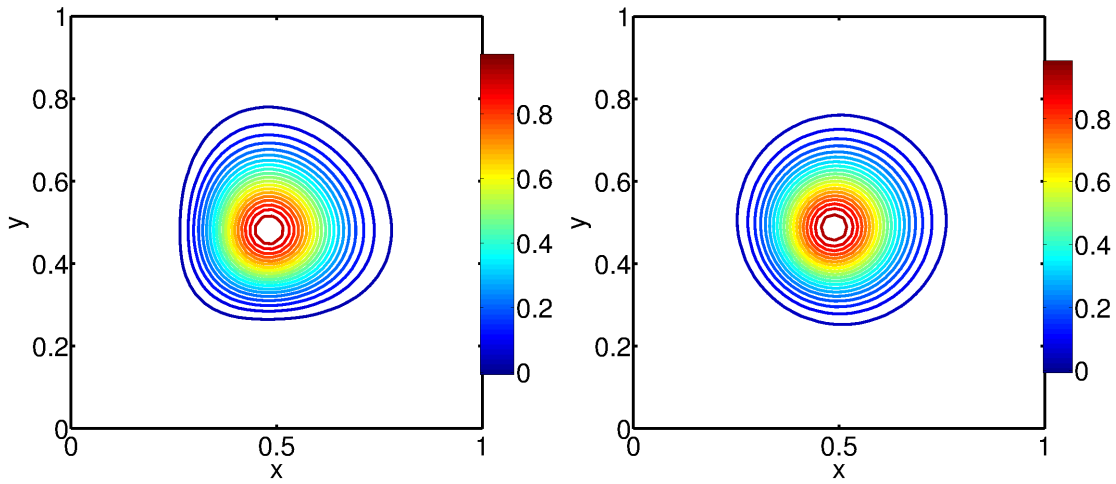

Figure 3.12: Evolution of 2D Gaussian function at time = 1 for standard MacCormack method(Left) and isotropic MacCormack(Right).

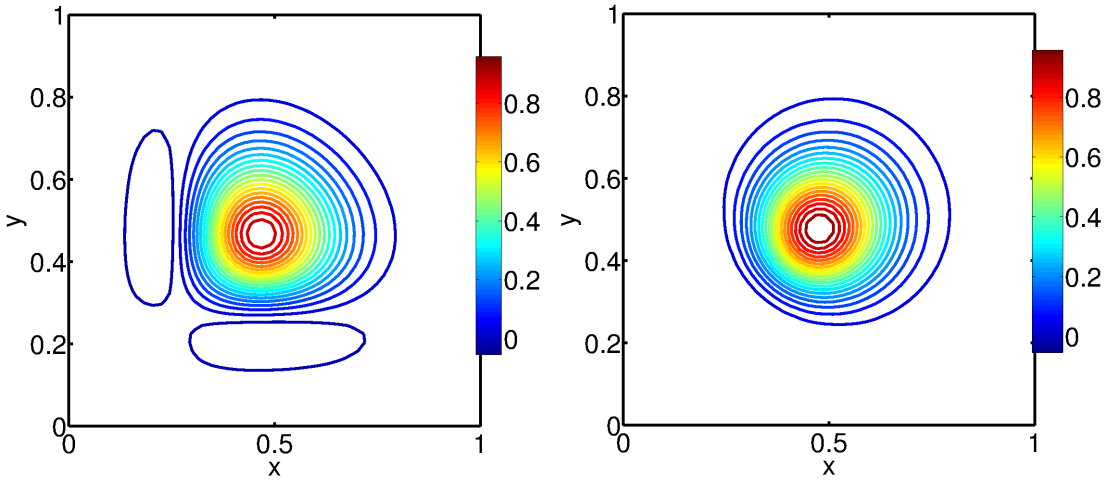

Figure 3.13: Evolution of 2D Gaussian function at time = 2 for standard MacCormack method(Left) and isotropic MacCormack(Right).

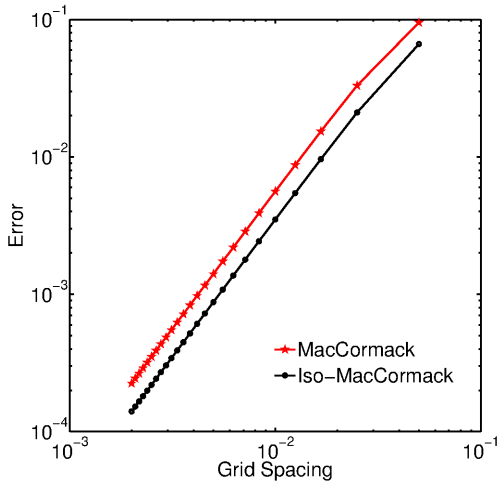

Figure 3.14: L^2-norm error *vs* grid spacing for standard MacCormack and Isotropic MacCormack method at time = 1. Here MacCormack is standard MacCormack method and Iso-MacCormack is isotropic MacCormack method.

3.4 Discrete Scheme for Diffusion Equation

In this section, the discretization of the diffusion equation is presented. In this thesis, the time discretization used for solving diffusion equation is

$$\frac{u_{i,j}^{n+1} - u_{i,j}^{n}}{\Delta t} = \tilde{\nabla}^2 u_{i,j}^{n}, \tag{3.34}$$

where $\tilde{\nabla}^2$ denotes the discrete laplacian.

We consider 2D gaussian function with variance 0.001 as initial condition on a 30×30 grid to solve the diffusion equation using CD2 and RL2 operators. The evolution of 2D gaussian at $time = 5$ using CD2 and RL2 and exact solution is shown in Fig. 3.15

It is evident from the plot that the accuarcy and isotropy of the RL2 operator is better compared to the CD2 operator.

3.5 Wave Equation Solver on Replica Grid

In this section, time discretization of wave equation with isotropic laplacian operator is presented. In order to do so, we write wave equation as a system of first order equations:

$$\frac{\partial P}{\partial t} = V \tag{3.35}$$

$$\frac{\partial V}{\partial t} = c_s^2 \left(\frac{\partial^2 P}{\partial x^2} + \frac{\partial^2 P}{\partial y^2} \right). \tag{3.36}$$

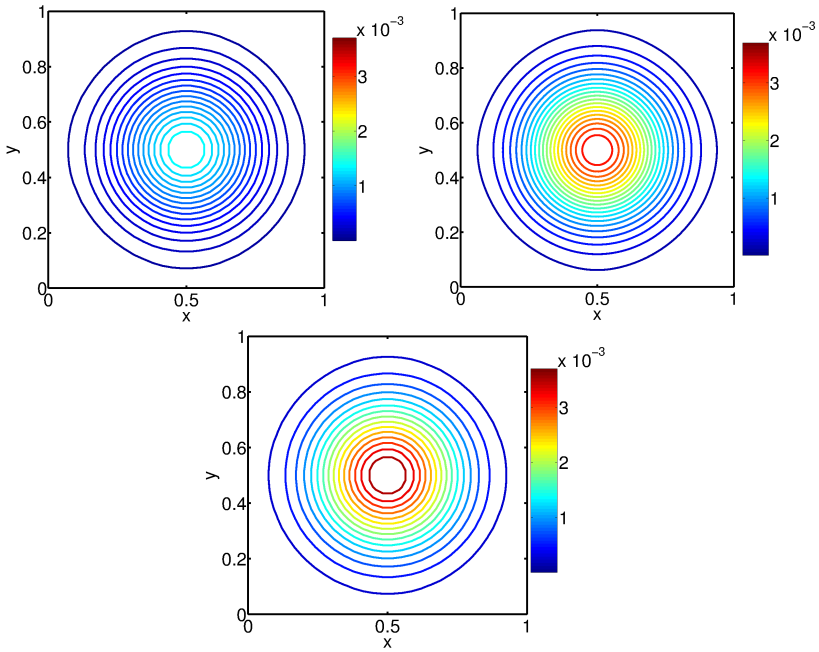

Figure 3.15: Diffusion of 2D gaussian function at $time = 5$ for CD2(Top left), exact(Top Right) and RL2 operator (Bottom). Here the diffusivity is taken as 0.01.

In this thesis, for solving wave equation we use backward difference in time for Eq. 3.35 and forward difference in time for Eq. 3.36.

$$\begin{aligned} \frac{P_{i,j}^{n+1} - P_{i,j}^{n}}{\Delta t} &= V_{i,j}^{n+1} \\ \frac{V_{i,j}^{n+1} - V_{i,j}^{n}}{\Delta t} &= c_s^2 \, \widetilde{\nabla}^2 P_{i,j}^{n}. \end{aligned} \tag{3.37}$$

where $\widetilde{\nabla}^2$ denotes appropriate discrete expression for the laplacian. The dispersion relation for the central difference and replica schemes with this time integration scheme are as follows:

$$\begin{aligned} \cos\left(\omega^{\mathrm{CD2}}\Delta t\right) &= 1 - \left(\frac{c_s \Delta t}{\Delta x}\right)^2 (2 - \cos(k_x \Delta x) - \cos(k_y \Delta y)), \\ \cos\left(\omega^{\mathrm{RL2}}\Delta t\right) &= 1 - \left(\frac{c_s \Delta t}{\Delta x}\right)^2 \frac{2}{3} \left[10 - \cos(k_x \Delta x) - \cos(k_y \Delta y) - 8\cos\left(\frac{k_x \Delta x}{2}\right)\cos\left(\frac{k_y \Delta y}{2}\right)\right]. \end{aligned} \tag{3.38}$$

In Fig. 3.16, the normalized dispersion relation for CD2 solution is shown via polar plot for different number of points per wavelength(N_λ). Here the radius of the plot is normalized by the exact solution given in the Eq. 3.14. It is evident that the dispersion relation is not isotropic, (i.e), and $N_\lambda = 16$ is atleast needed to get a reasonable answer. In Fig. 3.17 the polar plot of the dispersion relation for various second order and fourth order schemes such as RL2, RL4, CD2 and CD4 along with the exact solution is reported. It is evident that both second and fourth order replica schemes are reasonable for $N_\lambda = 8$. Furthermore, even for very low resolution ($N_\lambda = 4$), the RL2 and RL4 schemes are isotropic. Thus, the number of points required per wave length to get an isotropic profile is very less for the lattice based methods

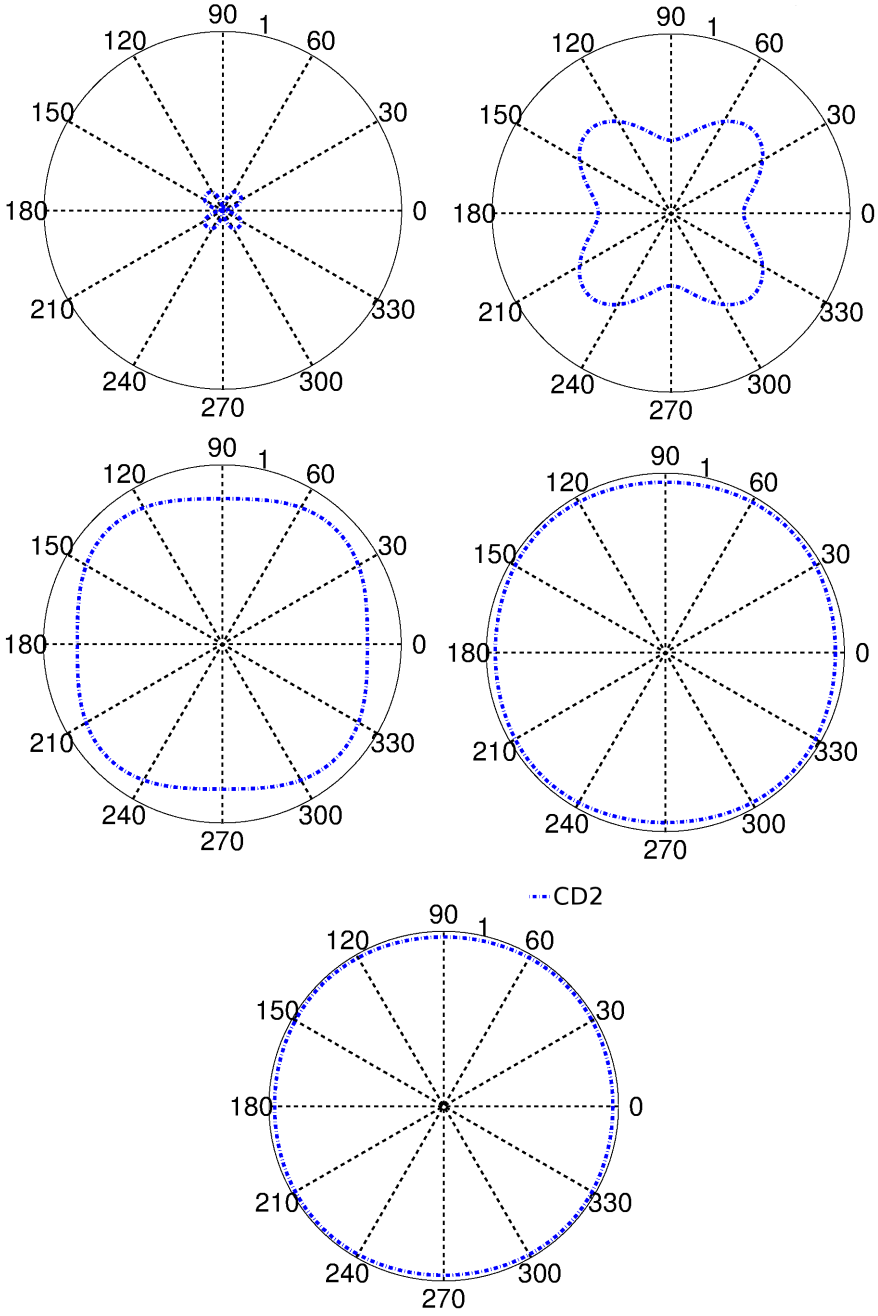

Figure 3.16: polar plot of the dispersion relation for CD2. Here the number of points per wavelength N_λ is taken as 2(Top Left) 4 (TopRight), 8(Middle left), 16 (Middle Right) and 20(Bottom)

scheme	Dispersion relation in low wave number limit
Exact	$\left(\frac{\omega}{c_s}\right)^2 = k^2$
CD2	$\left(\frac{\omega}{c_s}\right)^2 = k^2 - \frac{k^4c^2}{12}\left\{1 - \frac{\sin^2(2\theta)}{2}\right\}$
L2	$\left(\frac{\omega}{c_s}\right)^2 = k^2 - \frac{1}{12}k^4c^2$
RL2	$\left(\frac{\omega}{c_s}\right)^2 = k^2 - \frac{1}{24}k^4c^2$

Table 3.1: Dispersion relation for 2D scalar wave equation for different schemes in the low wave number limit, where $\Delta x = \Delta y = c$ and $k_x = k\cos\theta$ and $k_y = k\sin\theta$.

compared to the central operators. This trend can also be seen from low wave number limit of the dispersion relation reported in Table. 3.1. From this table it is evident that among all second order alternates, current scheme is most accurate as well as most isotropic. Here, reader is reminded that for many application related to real time visualization qualitative agreement with poor resolution is quite important(Enright *et al.* 2002; Foster & Fedkiw 2001; Nguyen *et al.* 2002; Foster & Metaxas 1996).

Next, we investigate the phase velocity and group veloicty for both schemes. The expressions for the group and phase velocities for the second order central difference scheme (CD2) is given by (Alford *et al.* 1974):

$$\frac{c^{\text{group, CD2}}}{c_s} = \frac{\left\{\sin\left(\frac{\pi\cos\theta}{N_\lambda}\right)\cos\left(\frac{\pi\cos\theta}{N_\lambda}\right)\cos\theta + \sin\left(\frac{\pi\sin\theta}{N_\lambda}\right)\cos\left(\frac{\pi\sin\theta}{N_\lambda}\right)\sin\theta\right\}}{\left\{1 - s^2\sin^2\left(\frac{\pi\cos\theta}{N_\lambda}\right) - s^2\sin^2\left(\frac{\pi\sin\theta}{N_\lambda}\right)\right\}^{1/2}\left\{\sin^2\left(\frac{\pi\cos\theta}{N_\lambda}\right) + \sin^2\left(\frac{\pi\sin\theta}{N_\lambda}\right)\right\}^{1/2}} \tag{3.39}$$

$$\frac{c^{\text{group, CD2}}}{c_s} = \frac{N_\lambda}{\pi s}\sin^{-1}\left[s\left\{\sin^2\left(\frac{\pi\cos\theta}{N_\lambda}\right) + \sin^2\left(\frac{\pi\sin\theta}{N_\lambda}\right)\right\}^{1/2}\right] \tag{3.40}$$

where $s = \frac{c_s\Delta t}{\Delta x}$ and N_λ is the number of points per wave length and $kh = 2\pi/N_\lambda$ and .

The expressions for the group and phase velocities using the Eqs. (3.4 - 3.3) for replica method RL2 is:

$$\begin{aligned}\frac{c^{\text{group, RL2}}}{c} &= \frac{1}{\sqrt(6)\left\{1 - \frac{s^2}{6}G\right\}^{1/2}G^{1/2}}\left\{\sin\left(\frac{2\pi\cos\theta}{N_\lambda}\right)\cos\theta + \sin\left(\frac{2\pi\sin\theta}{N_\lambda}\right)\sin\theta\right. \\ &+ \left. 4\sin\left(\frac{\pi\cos\theta}{N_\lambda}\right)\cos\left(\frac{\pi\sin\theta}{N_\lambda}\right)\cos\theta + 4\sin\left(\frac{\pi\sin\theta}{N_\lambda}\right)\cos\left(\frac{\pi\cos\theta}{N_\lambda}\right)\sin\theta\right\}\end{aligned} \tag{3.41}$$

$$\frac{c\text{phase, RL2}}{c} = \frac{N_\lambda}{\pi s}\sin^{-1}\left[\frac{s}{\sqrt(6)}G^{1/2}\right]. \tag{3.42}$$

where $G = 10 - \cos\left(\frac{2\pi\cos\theta}{N_\lambda}\right) - \cos\left(\frac{2\pi\sin\theta}{N_\lambda}\right) - 8\cos\left(\frac{\pi\cos\theta}{N_\lambda}\right)\cos\left(\frac{\pi\sin\theta}{N_\lambda}\right)$.

It is evident from the Fig. 3.18 and Fig. 3.19, that at $\theta = 0^o$ both the phase velocity and the group velocities are deviating a lot for CD2 operator compared to $\theta = 45^o$. Furthermore, based on Fig. 3.18 and Fig. 3.19, one can claim that at all propagation angle the RL2 operator has better accuracy for phase and group velocities as compared to the CD2 operator.

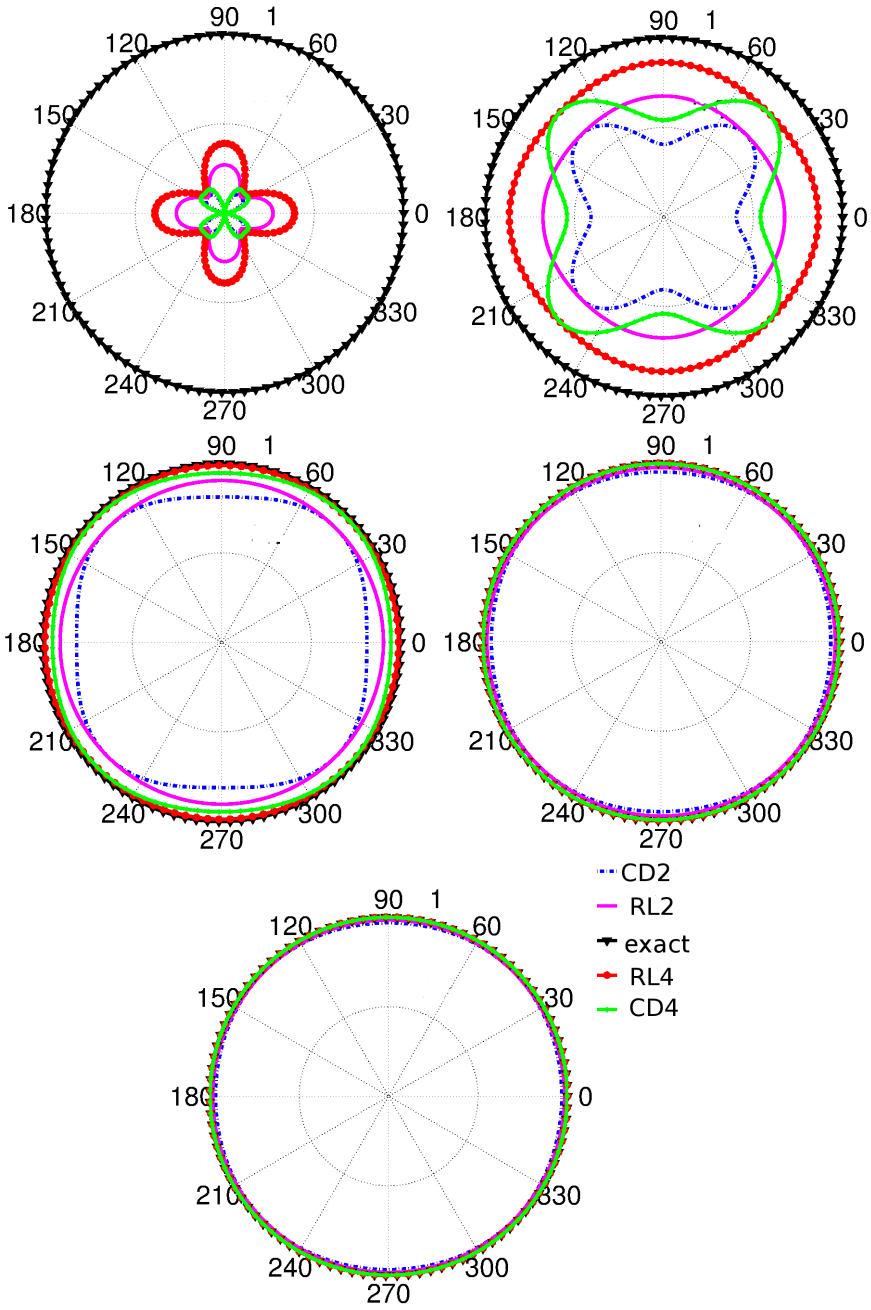

Figure 3.17: polar plot of the dispersion relation for the wave number for different schemes such as RL2, RL4, CD2 and CD4 along with the exact solution. Here the number of points per wavelength N_λ is taken as 2(Top Left) 4 (TopRight), 8(Middle left), 16 (Middle Right) and 20(Bottom)

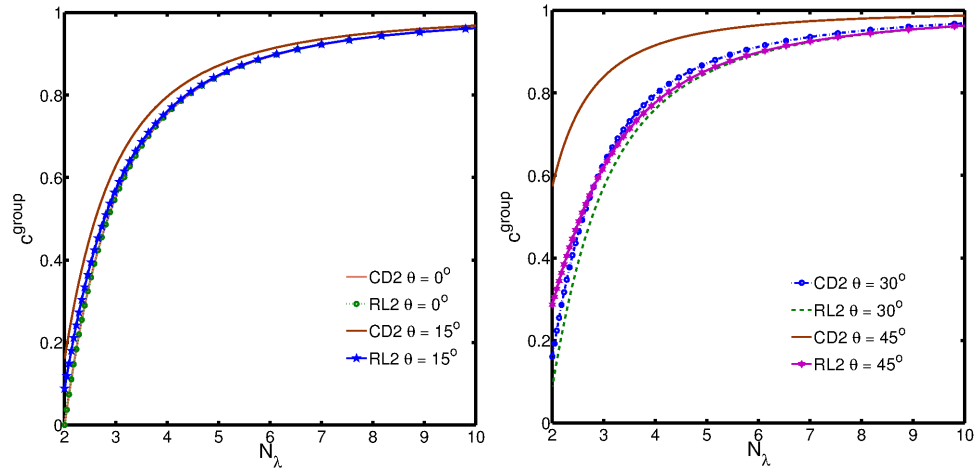

Figure 3.18: Plots for normalized group velocity for fully discrete wave equation using CD2 and RL2 operators at different angles of propagation.

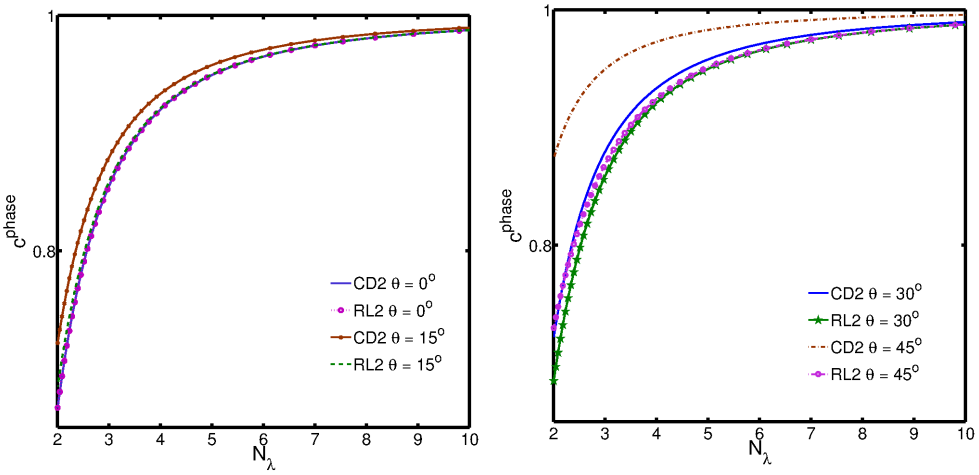

Figure 3.19: Plots for normalized phase velocity for fully discrete wave equation using CD2 and RL2 operators at different angles of propagation.

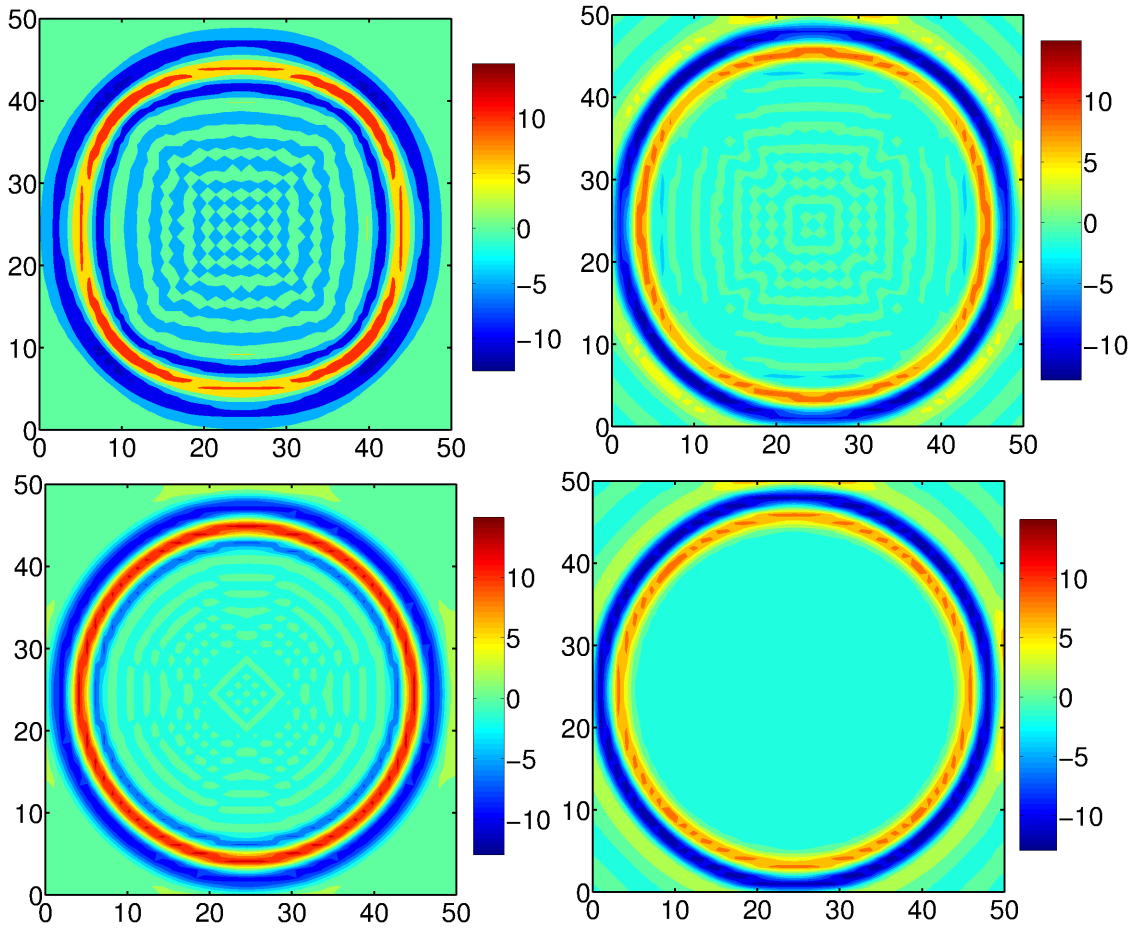

Figure 3.20: snap shots of ripples at $t = 0.05$ for different schemes CD2(Top Left), CD4 (Top Right), RL2(Bottom Left), RL4(Bottom Right).

3.5.1 Test Case: Simulation of Ripples

Finally, in order to test accuracy of the wave solver, simulation was performed with the source function in the form of a ricker wavelet(Alford *et al.* 1974; Schneider 2010).

$$S(t) = \left(1 - 2at^2\right) exp(-at^2), \tag{3.43}$$

where a is a constant. A square domain of 50X50 with source function at (25, 25) point in space was taken. Here the propagation speed c_s is taken as 300 and $a = 2$. At t = 0.05, the isocontours of the pressure are plotted and the same are reported in the Fig. 3.20.

It is evident from the Fig. 3.20 that the ripples simulated CD2 and CD4 are not isotropic and the simulation using lattice schemes are isotropic. So, if operators which are not isotropic are considered for discretization of such problems, the actual characteristics of the problem will not be reflected in the simulation.

We considered the same ricker wavelet with$a = 2$ as in Eq. 3.43 at a point (1000,1000) with $c_s = 1500$ on a square domain of 2000X2000 and the pressure variations are recorded at six different points using CD4 and RL4 by varying the grid spacing.

In Figs.(3.21 -3.26), the time evolution of pressure for methods CD4, RL4 at six different points (1212,1212), (1260,1150), (1424,1424), (1300,1600), (1600,1100) and (1520,1300) is re-

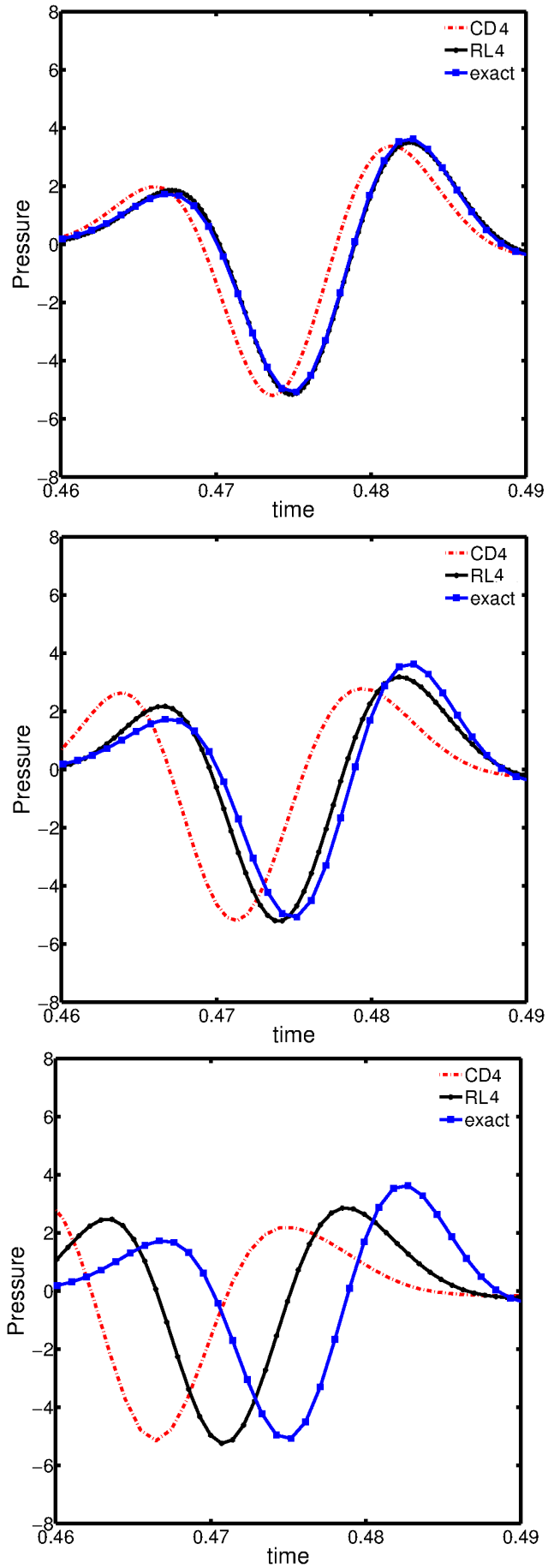

Figure 3.21: Time evolution of pressure for different methods CD4, RL4 at a point (1300,1600). Here the grid spacing(dx) is taken as 1(Top), 2(Middle) and 3(Bottom).

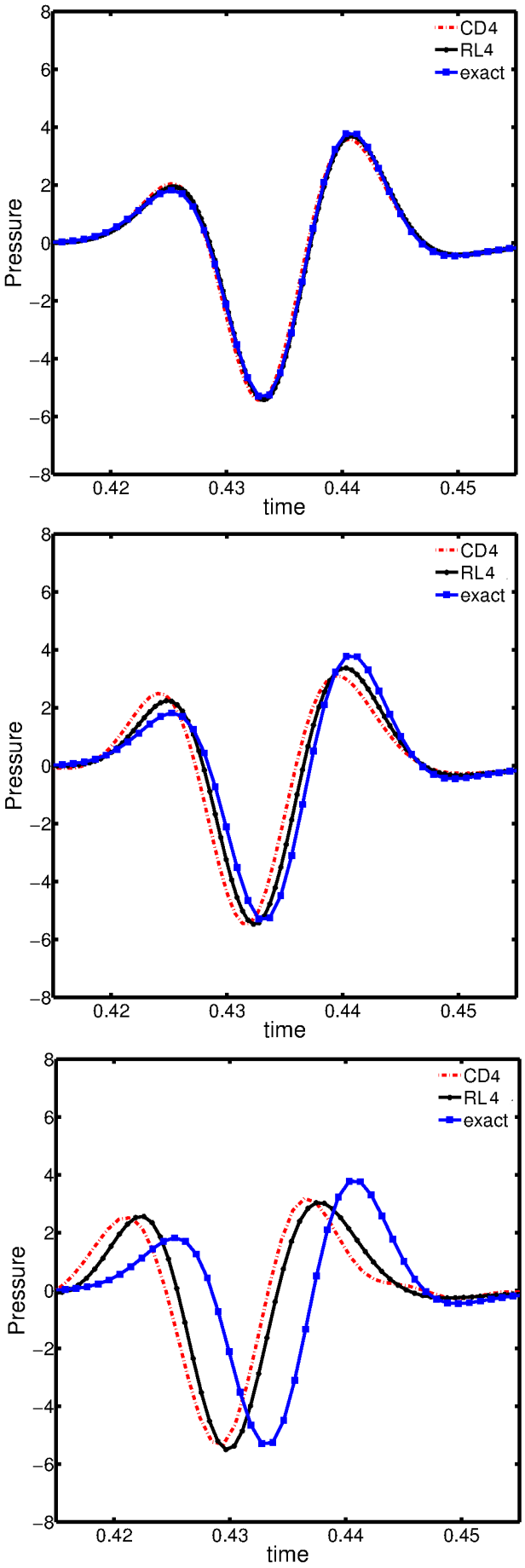

Figure 3.22: Time evolution of pressure for different methods CD4, RL4 at a point (1600,1100). Here the grid spacing(dx) is taken as 1(Top), 2(Middle) and 3(Bottom).

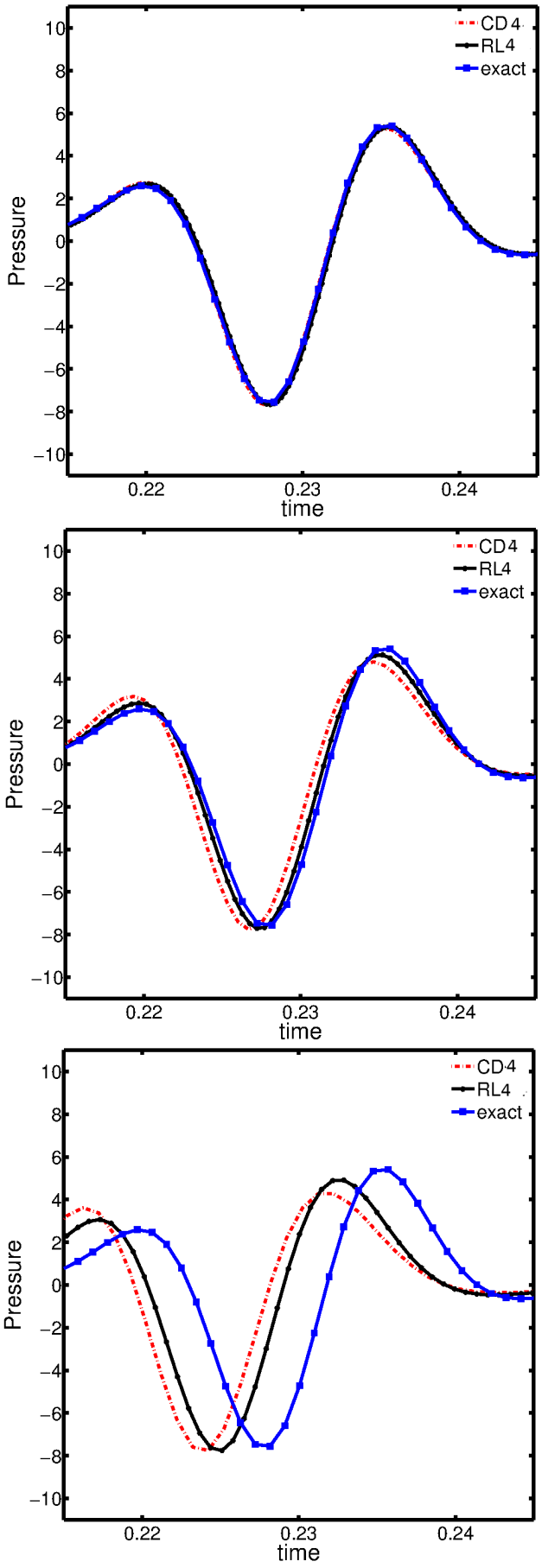

Figure 3.23: Time evolution of pressure for different methods CD4, RL4 at a point (1260,1150). Here the grid spacing(dx) is taken as 1(Top), 2(Middle) and 3(Bottom).

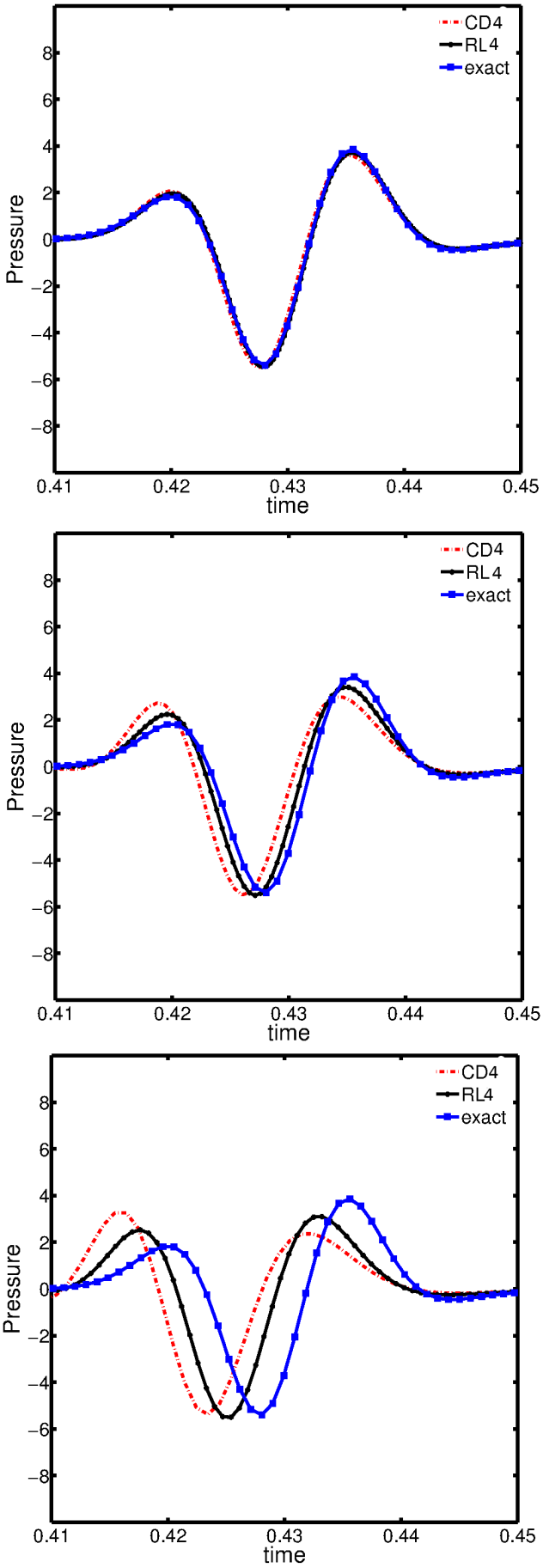

Figure 3.24: Time evolution of pressure for different methods CD4, RL4 at a point (1520,1300). Here the grid spacing(dx) is taken as 1(Top), 2(Middle) and 3(Bottom).

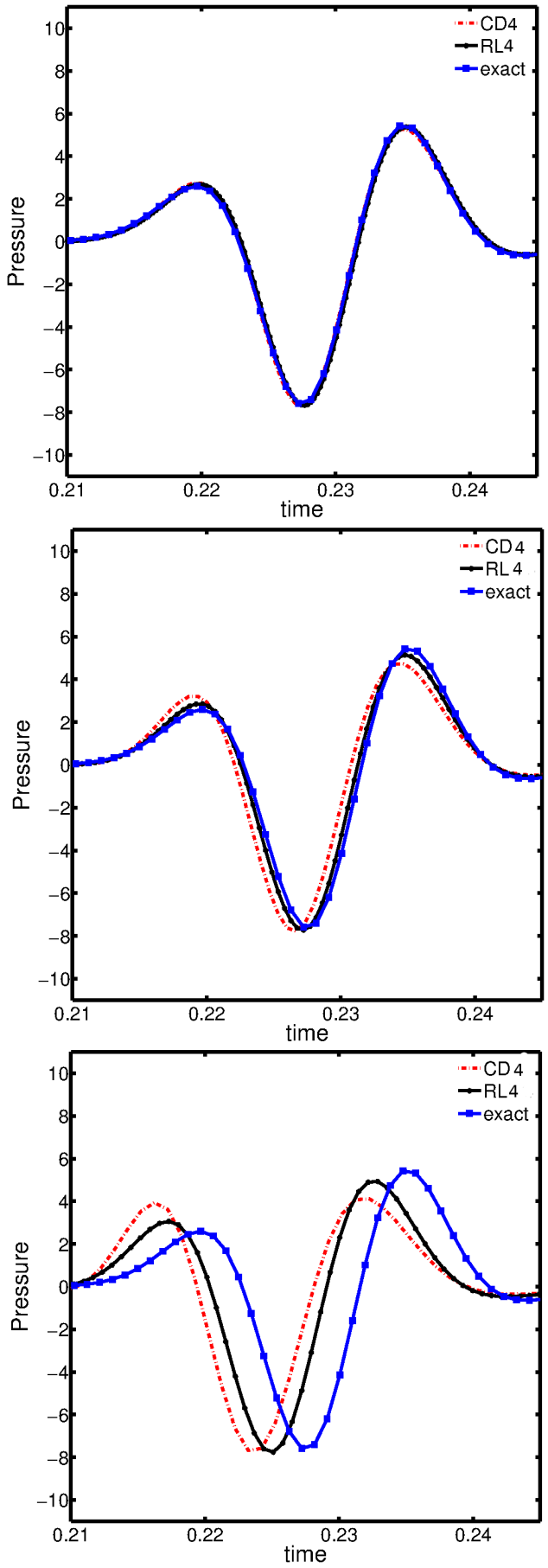

Figure 3.25: Time evolution of pressure for different methods CD4, RL4 at a point (1212,1212). Here the grid spacing(dx) is taken as 1(Top), 2(Middle) and 3(Bottom).

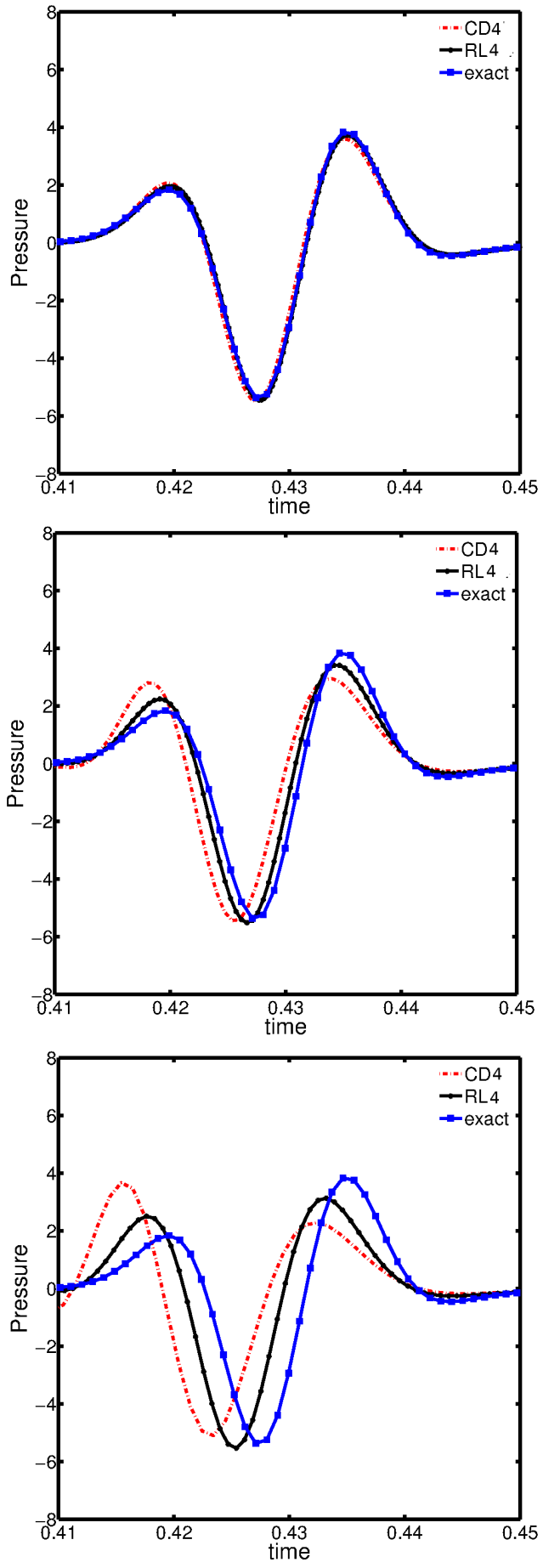

Figure 3.26: Time evolution of pressure for different methods CD4, RL4 at a point (1424,1424). Here the grid spacing(dx) is taken as 1(Top), 2(Middle) and 3(Bottom).

ported. Here the grid spacing(dx) is taken as $1, 2$ and 3. These results are compared with the exact solution. It is evident from the figure that the RL4 methods coincided with the exact solution in most of the cases compared to the CD4. It is also clear from these figures that the phase error for the RL4 scheme is less compared to the CD4 scheme.

In Fig. 3.27, the time evolution of pressure for methods RL4 with $dx = 2$ and CD4 with $dx = 1.5$ and $dx = 2$ is compared with the exact solution. In most of these plots CD4 at $dx = 1.5$ coincided with RL4 at $dx = 2$ which shows the accuracy of the RL4 scheme over the CD4 scheme.

Thus, it can be concluded that the replica lattice schemes are very effective in reducing the error as well as retaining the isotropic characteristics of the original problem.

3.6 Maxwell Equations

As final example, we consider Maxwell equations describing electromagnetic wave equation (Griffiths & College 1999; Jackson 1999).

$$\begin{aligned} \mu\partial_t \mathbf{H} &= -\boldsymbol{\nabla} \times \mathbf{E}, \\ \epsilon\partial_t \mathbf{E} &= \mu\boldsymbol{\nabla} \times \mathbf{H}, \\ \boldsymbol{\nabla} \cdot \mathbf{E} &= 0, \\ \boldsymbol{\nabla} \cdot \mathbf{B} &= 0, \end{aligned} \tag{3.44}$$

where $\mathbf{H}$ is the magnetic field, $\mathbf{E}$ is the Electric field, μ is magnetic permeability, $\mathbf{B} = \mu\mathbf{H}$ and ϵ is the electric permittivity. Maxwell equations can be rewritten in the form of vector wave equation for electric field as:

$$\frac{\partial^2 \mathbf{E}}{\partial t^2} = \frac{1}{\mu\epsilon}\nabla^2 \mathbf{E}. \tag{3.45}$$

Finite difference time domain method(FDTD) (Yee 1966; Yefet & Petropoulos 2001; Young *et al.* 1997; Xie *et al.* 2002; Gilles *et al.* 2000) is one of the most widely used method to solve the Maxwell equations. In this method, one uses a version of staggered grid, called Yee's grid, to define the electric and magnetic fields (See Fig.3.28 for grid arrangement in 2-D). As shown in Fig.3.28, for 2D case, the secondary and tertiary grids are displaced by half the grid spacing x and y directions respectively. As an example if we consider a transverse magnetic mode (TM) (Griffiths & College 1999; Jackson 1999)the electric field, E_z is defined on the primary grid and the magnetic fields H_x and H_y are defined on the secondary and tertiary grids respectively. In this method the partial derivatives are discretized by using the standard central difference of second order on staggered grid. For example , x derivative of any quantity ϕ is approximated as

$$\partial_x \phi \sim \frac{\phi_{i+1/2,j} - \phi_{i-1/2,j}}{\Delta x}. \tag{3.46}$$

As discussed in Chap. 2, that the standard central difference (CD) operators are not isotropic, the Yee scheme which uses the CD operators cannot be isotropic. Later hexagonal grids were proposed by Liu (Liu 1996) which has less numerical phase space anisotropy compared to the Yee grid.

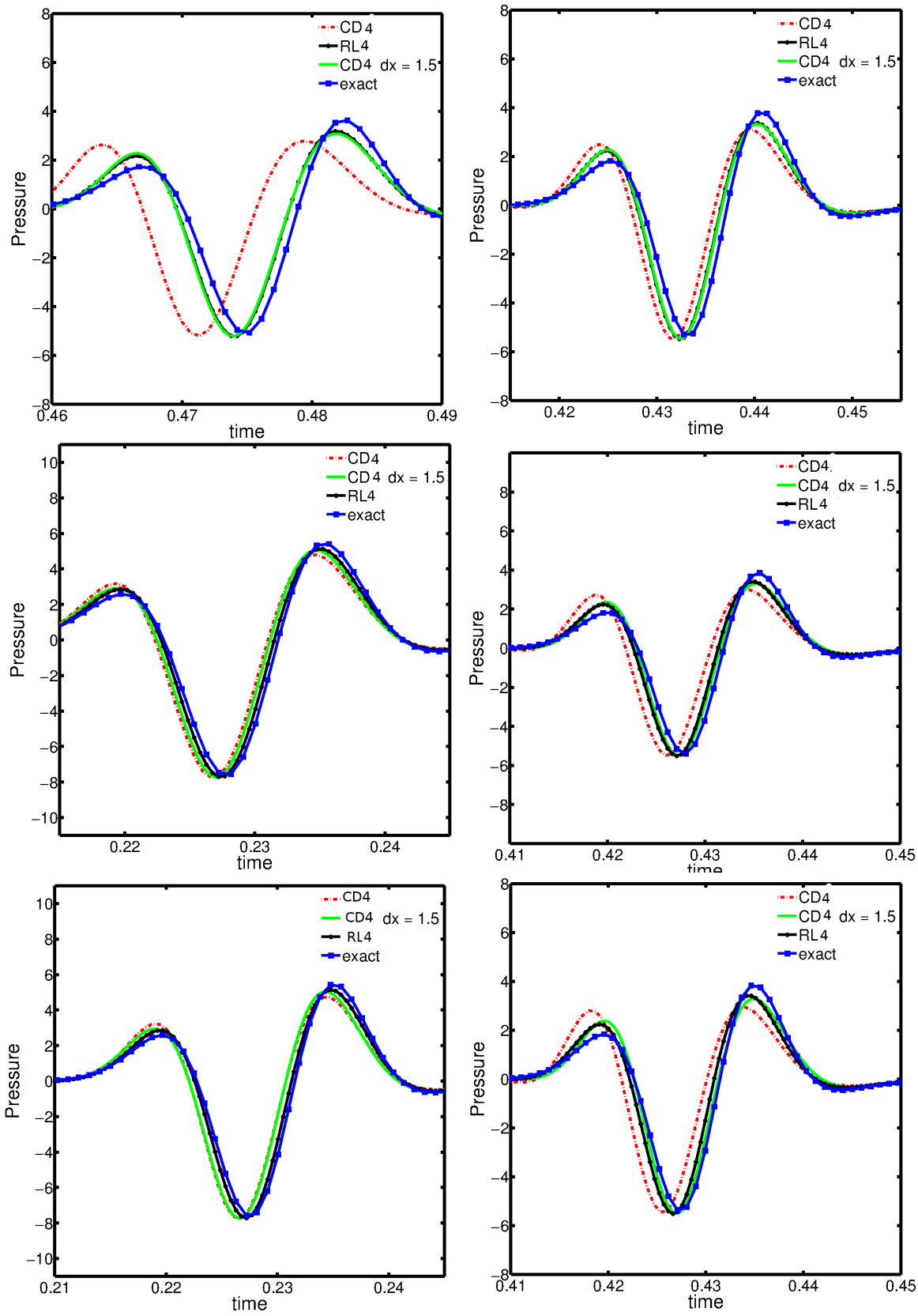

Figure 3.27: Time evolution of pressure for different methods CD4 with $dx = 1.5$ and $dx = 2$ and RL4 with $dx = 2$ at a six sensor locations (1300,1600)(Top Left), (1600,1100)(Top Right), (1260,1150)(Middle Left),(1520,1300)(Middle Right), (1212,1212)(Bottom Left) and (1424,1424)(Bottom Right).

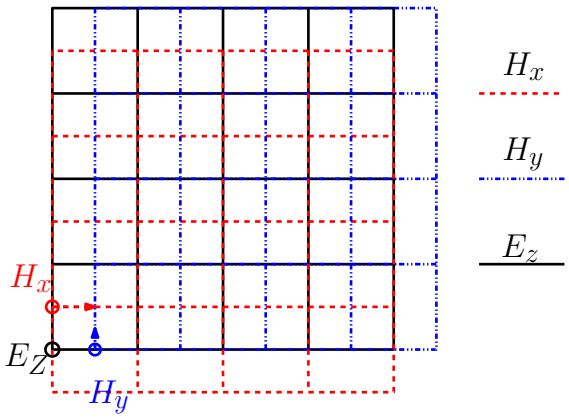

Figure 3.28: Yee grid. Here black represents primary grid and blue and red lines represents the secondary and tertiary grids respectively.

In this section, the dispersion relation of the Eq. 3.45 is derived and the isotropy of the scheme is verified with replica lattice operators.

Transverse Magnetic Modes

As an example consider maxwell Equations for TM modes(Taflove & Hagness 2000), which correspond to setting:

$$B_x = B_y = 0, \qquad E_z = 0, \tag{3.47}$$

The time derivatives are discretized using the standard central difference. For example the discrete derivative at $n + 1/2$ time level is calaculated as

$$\tilde{\partial}_t \phi|_{i,j}^{n+1/2} \sim \frac{\phi_{i,j}^{n+1} - \phi_{i,j}^{n}}{\Delta t} + O(\Delta t)^2. \tag{3.48}$$

In this thesis, the discretization of the Maxwell equations is done in the form of

$$\begin{aligned} \mu \tilde{\partial}_t \mathbf{H}|_{i,j}^{n+1} &= -\tilde{\boldsymbol{\nabla}} \times \mathbf{E}|_{i,j}^{n}, \\ \epsilon \tilde{\partial}_t \mathbf{E}|_{i,j}^{n+1/2} &= \mu \tilde{\boldsymbol{\nabla}} \times \mathbf{H}|_{i,j}^{n-1/2}, \end{aligned} \tag{3.49}$$

For this case, Eq. 3.44 when discretized using the Yee scheme can be expressed as:

$$\hat{\mathbf{a}}_{i,j}^{n+1} = \mathbf{G} \hat{\mathbf{a}}_{i,j}^{n}, \tag{3.50}$$

where $\mathbf{G}$ is the amplication matrixand $\hat{a}_{i,j}^{n} = [H_x^{n-1/2} \; H_y^{n-1/2} \; E_z^{n}]$.

$$\begin{bmatrix} H_x^{n+1/2} \\ H_y^{n+1/2} \\ E_z^{n+1} \end{bmatrix} = \begin{bmatrix} S_t & 0 & \chi_y S_y \\ 0 & S_t & -\chi_x S_x \\ \eta_y S_y C_x & -\eta_x S_x C_y & S_t \end{bmatrix} \begin{bmatrix} H_x^{n-1/2} \\ H_y^{n-1/2} \\ E_z^{n} \end{bmatrix}$$

where $S_t = sin(\omega \Delta t/2)$, $S_x = sin(k_x \Delta x)$, $C_y = cos(k_y \Delta y)$ and $\eta_x = \frac{\Delta t}{\epsilon \Delta x}, \chi_x = \frac{\Delta t}{\mu \Delta x}$. The

dispersion relation for the Yee scheme in this case is:

$$S_t^2 = (c\Delta t)^2 \left\{ \left(\frac{S_{x/2}}{\Delta x} \right)^2 + \left(\frac{S_{y/2}}{\Delta y} \right)^2 \right\}. \tag{3.51}$$

In low wave number limit the Eq.(3.51) transforms to:

$$\left(\frac{\omega}{c_s} \right)^2 = k^2 - \frac{k^4 c^2}{12} \left\{ 1 - 2\cos^2\theta \sin^2\theta \right\} + \cdots . \tag{3.52}$$

It is evident from Eq. 3.51, that in low wave number limit, the method is quite accurate but the error is not isotropic,(i.e) it has dependence on the angle of rotation(Panaretos *et al.* 2007).

In Fig. 3.28, the dispersion relation for yee scheme is plotted on a polar plot for different number of points per wavelength(N_λ). The radius of the polar plot is normalized using the exact solution. It is evident from the figure that when resolution is moderate $N_\lambda = 4$, the isotropic error is very high, (i.e) at different angles of rotation, the values of the normalized dispersion relation is different.

3.6.1 Replica Lattice Scheme

As we know that the accuracy of the replica schemes is better than the standard lattice schemes we use the replica to solve the Maxwell equations.

As already discussed in the Sec. 3.2 the replica scheme has two grids one displaced by half the grid size in all the dimensions considered and variables are defined on all the grids. Replica grid has the advantages of both the staggered and unstaggered grids. The error for second order replica scheme is $\left(\frac{\Delta x}{\sqrt{(2)}} \right)^2$.

Dispersion Relation

The maxwell Eqs. 3.47 using the lattice curl scheme with replica D2Q9 weights when taken in fourier mode, the dispersion relation will be of the form:

$$S_t^2 = \left(\frac{c_s \Delta t}{6\Delta x} \right)^2 \left\{ (S_x^2 + S_y^2) + 16(S_{x/2}^2 C_{y/2}^2 + C_{x/2}^2 S_{y/2}^2 + S_{x/2}^2 C_{x/2} C_{y/2} + S_{y/2}^2 C_{x/2} C_{y/2}) \right\}, \tag{3.53}$$

where $c = \frac{1}{\sqrt{\mu\epsilon}}$ is the speed of light in the material being modelled.

When low wave number limit is considered Eq.(3.53) transforms to:

$$\left(\frac{\omega}{c_s} \right)^2 = k^2 - \frac{1}{6} k^4 (\Delta x)^2 + \cdots . \tag{3.54}$$

It is evident from the Eqs. 3.52 and 3.54, that the dispersion relation for the replica second order scheme approaches that of the exact in the low wave number limit. The error of the replica scheme as compared to the Yee scheme is still high but the error is isotropic in nature unlike the Yee scheme.

In Fig. 3.30, the dispersion relation for the replica lattice scheme of second order (RL2) and

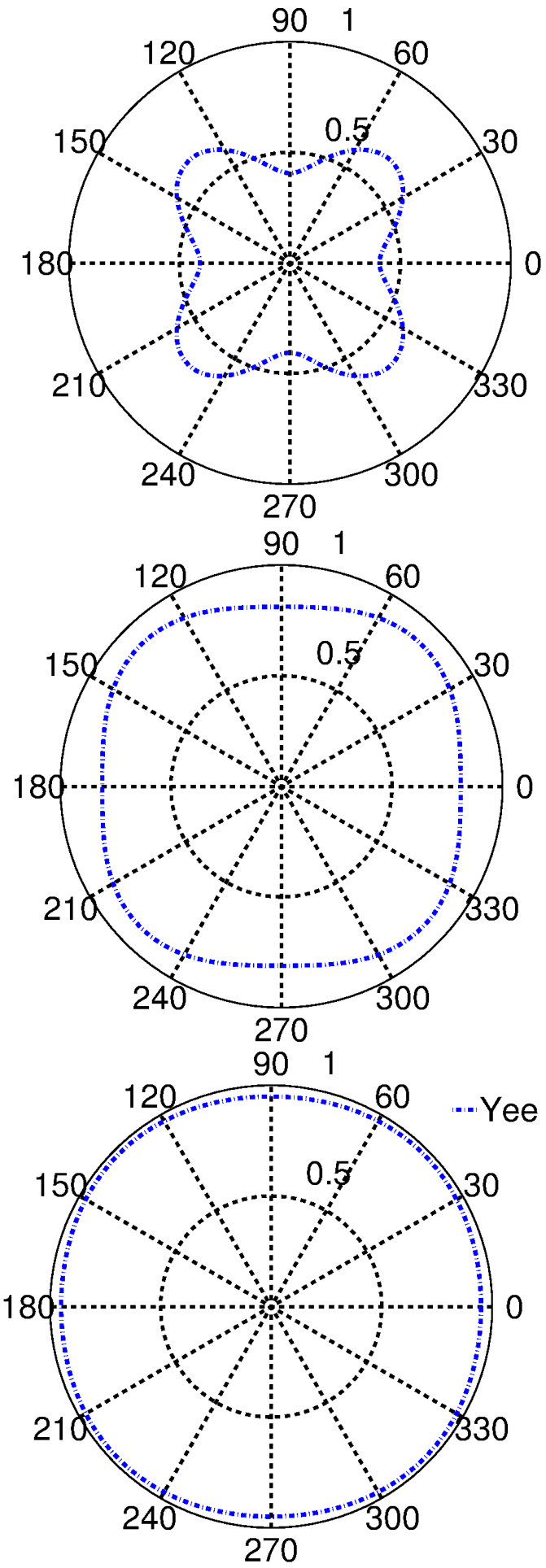

Figure 3.29: Polar plot of dispersion relation using the Yee scheme . Here the radius of the polar plot is $\left(\frac{\omega}{c_s\ k}\right)^2$ and number of points per wavelength(N_λ) as 4(Top),8(Middle) and 16(Bottom).

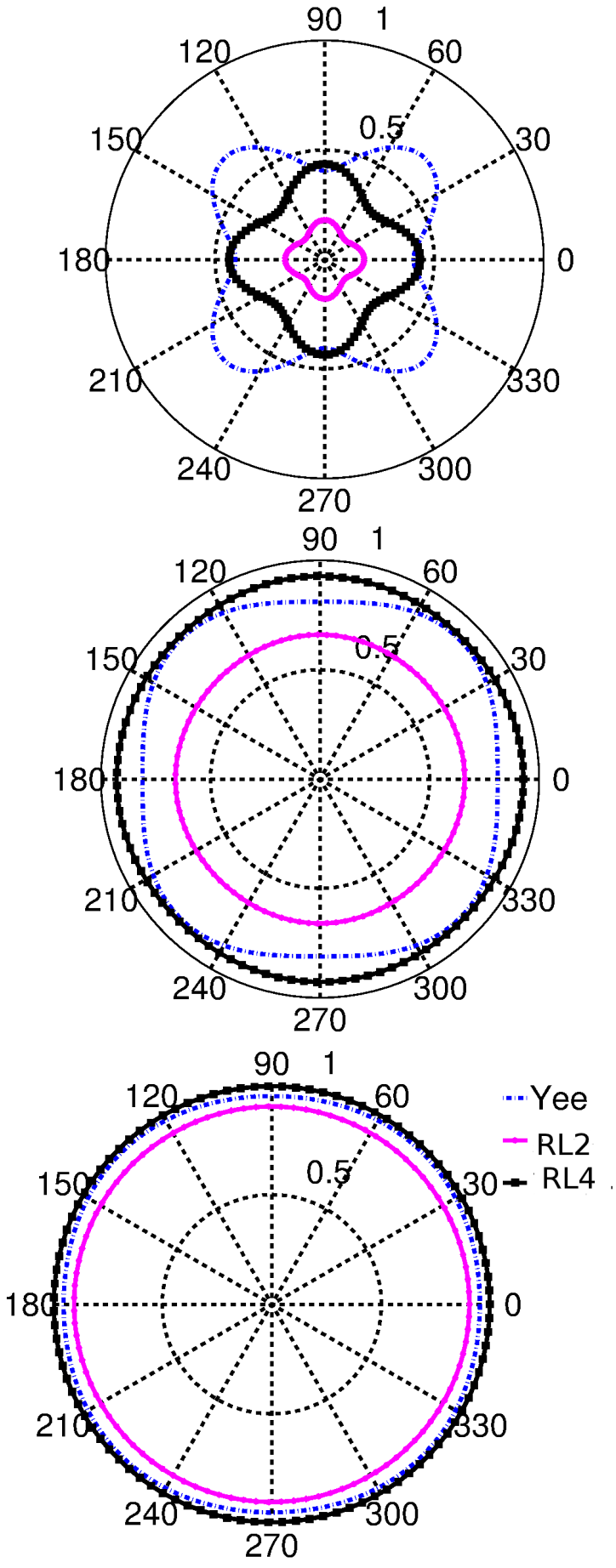

Figure 3.30: Polar plot of dispersion relation using the Yee scheme and the replica lattice scheme Eq. 3.53. Here the radius of the polar plot is $\left(\frac{\omega}{c_s\ k}\right)^2$ and number of points per wavelength(N_λ) as 4(Top),8(Middle) and 16(Bottom).

replica scheme of fourth order(RL4)and that of Yee scheme is plotted for different number of points per wavelength. The radius of the plot is normalized by the exact dispersion relation. It is evident from the figure that the error for the RL2 is high compared to the Yee scheme but it becomes isotropic at few number of points per wavelength. The RL4 scheme has low error comnpared to the Yee scheme and it becomes isotropic even with few number of points per wavelength.

Testcase

To validated the formulations, consider a square domain of length 2π with the initial conditions as follows (Yefet & Petropoulos 2001):

$$\begin{aligned} E_z(x,y,0) &= \cos(k_x x)\cos(k_y y), \\ H_x(x,y,0) &= \frac{k_y}{\omega}\cos(k_x x)\sin(k_y y), \\ H_y(x,y,0) &= -\frac{k_x}{\omega}\sin(k_x x)\cos(k_y y), \end{aligned}$$

where $\omega = \sqrt{k_x^2 + k_y^2}$.

The boundary conditions for electric field are:

$$\begin{aligned} E_z(0,y,t) &= \cos(k_y y)\cos(\omega t), \\ E_z(1,y,t) &= \cos(k_x)\cos(k_y y)\cos(\omega t), \\ E_z(x,0,t) &= \cos(k_x x)\cos(\omega t), \\ E_z(x,1,t) &= \cos(k_x x)\cos(k_y)\cos(\omega t). \end{aligned}$$

The boundary conditions for magnetic field are:

$$\begin{aligned} H_x(0,y,t) &= \frac{k_y}{\omega}\sin(k_y y)\sin(\omega t) \\ H_y(0,y,t) &= 0 \\ H_x(1,y,t) &= \frac{k_y}{\omega}\cos(k_x)\sin(k_y y)\sin(\omega t) \\ H_y(1,y,t) &= -\frac{k_x}{\omega}\sin(k_x)\cos(k_y y)\sin(\omega t) \\ H_x(x,0,t) &= 0 \\ H_y(x,0,t) &= -\frac{k_x}{\omega}\sin(k_x x)\sin(\omega t) \\ H_x(x,1,t) &= \frac{k_y}{\omega}\cos(k_x x)\sin(k_y)\sin(\omega t) \\ H_y(x,1,t) &= -\frac{k_x}{\omega}\sin(k_x x)\cos(k_y) sin(\omega t) \end{aligned}$$

Here, the exact solution for the test case is of the form:

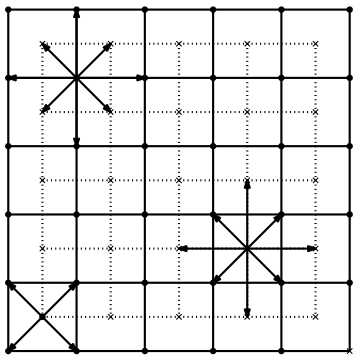

Figure 3.31: Replica grid with the replica D2Q9 and replica D2Q5 stencils.

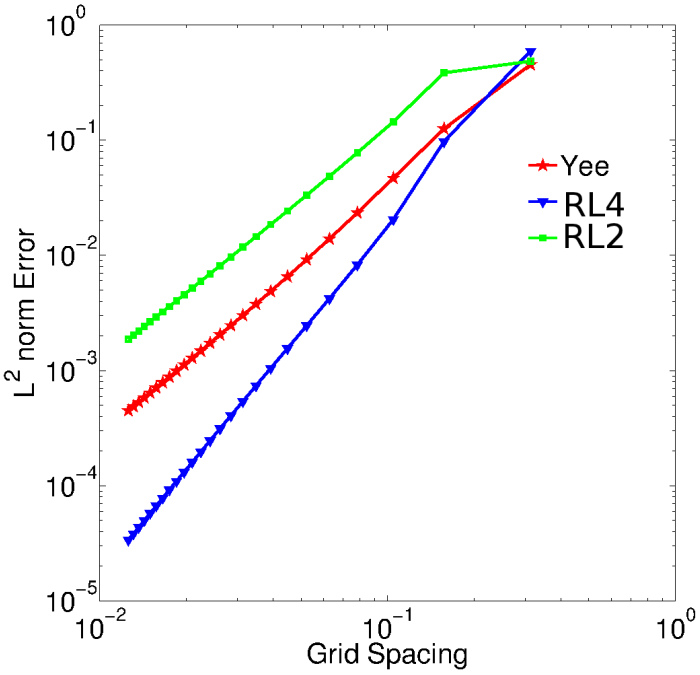

Figure 3.32: L^2 Norm *(vs)* grid spacing on a log-log plot.

$$E_z = \cos(k_x x)\cos(k_y y)\cos(\omega t)$$

Here we considered $k_x = 3$ and $k_y = 4$ and $\mu = \epsilon = 1$.

In Fig. 3.31, the replica D2Q9 stencil is used to carry out the computations in the interior nodes and at the boundaries we use a replica D2Q5 model shown the figure to calculate the curl. The weights for this lower model is calculated using the constraints defined in Chap. 2. Because, we use a lower model at the boundaries, there is no need of defining the boudary conditions for the magnetic field. So, it has the advantages of the staggered grid.

In Fig. 3.32, the L^2-norm of the electric field is plotted agianst the grid spacing on a log-log plot. It is evident from the figure that the RL4 has the best accuracy of all.

It is evident from the Fig. 3.33, that the error for the Yee scheme is very high compared to the RL4 lattice scheme.

In Table. 3.2, dispersion relation for all the schemes is reported. It is evident from the table that the Yee scheme is dependent on angle of rotation, whereas the lattice schemes are perfectly

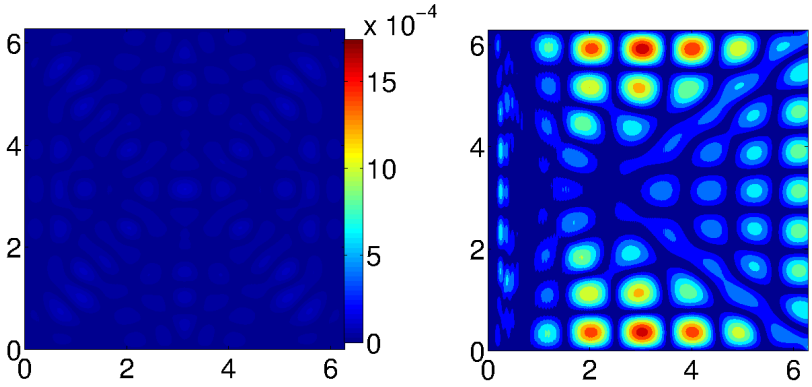

Figure 3.33: Isocontours of error in the electric field for both Yee scheme(right) and RLC4(left).

scheme	Dispersion relation in low wave number limit
Exact	$\left(\frac{\omega}{c_s}\right)^2 = k^2$
Yee	$\left(\frac{\omega}{c_s}\right)^2 = k^2 - \frac{k^4 c^2}{12}\left\{1 - 2\cos^2\theta\sin^2\theta\right\}$
L2	$\left(\frac{\omega}{c_s}\right)^2 = k^2 - \frac{1}{3}k^4 c^2$
RL2	$\left(\frac{\omega}{c_s}\right)^2 = k^2 - \frac{1}{6}k^4 c^2$

Table 3.2: Dispersion relation for different schemes in the low wave number limit.

isotropic.

3.7 Conclusions

Discrete isotropic operators formulated in the previous chapter were implemented succesfully for different PDEs such as advection, diffusion, wave and Maxwell equations. In most of the cases, the replica schemes have better accuracy compared to the standard centered difference schemes. Further, the number of points per wavelength required to have isotropy is very less for the replica schemes compared to the other standard schemes.

Chapter 4

Outlook

For finite difference operators on the uniform grid, discrete operations are generally restrained to the principal directions of the lattice (coordinate directions on a rectangular grid), often neglecting the grid points along other directions. In this thesis, an new formalism for creating discrete operators which retain as many symmetries as possible of their continuum counterparts is developed. It was shown that the problem of finding discrete operators which respect isotropy and symmetries of the continuous operator is analogous to finding discrete velocity models for which lower order moments of discrete equilibrium matches with that of Maxwell-Boltzmann distribution. Furthermore, it was shown that compact finite difference schemes can be formulated directly in multidimensional sense, provided the leading order error in discrete operators are isotropic. Finally, we generalize the concept of staggered grid to that of replica grid, where multiple copies of space filling lattices are introduced simultenously. These grids are obtained via translation of original grid by fixed amount and unlike staggered grid formulations, all variables are kept on all grids. We show that such replica grids coupled with isotropic operators provide an efficient alternate to existing finite difference methods.

Thes operators on replica grid was tested for a host of partial differential equations. It was shown that the method is efficient for linear advection equation, diffusion equation and wave equation. The results suggest that this new approach has potential to substantially improve the performance of the finite difference methods. However, a more careful and eloborate investigations are needed before method can emerge as an alternate to traditional approaches.

References

Alford, R., Kelly, K. & Boore, D. 1974 Accuracy of finite-difference modeling of the acoustic wave equation. *Geophysics* **39** (6), 834–842.

Arfken, G. B., Weber, H. J. & Harris, F. E. 2005 *Mathematical Methods For Physicists International Student Edition*. Access Online via Elsevier.

Bochev, P. B. & Hyman, J. M. 2006 Principles of mimetic discretizations of differential operators. In *Compatible spatial discretizations*, pp. 89–119. Springer.

Brillouinn, L. 1960 *Wave propagation and group velocity*. Academic Press Inc.

Canuto, C. G., Hussaini, M. Y. & Quarteroni, A. 2007 *Spectral methods: evolution to complex geometries and applications to fluid dynamics*. Springer.

Cheong, C. & Lee, S. 2001 Grid-optimized dispersion-relation-preserving schemes on general geometries for computational aeroacoustics. *Journal of Computational Physics* **174** (1), 248–276.

Chikatamarla, S. S. & Karlin, I. V. 2009 Lattices for the lattice boltzmann method. *Physical Review E* **79** (4), 046701.

Chung, T. 2010 *Computational fluid dynamics*. Cambridge university press.

Enright, D., Marschner, S. & Fedkiw, R. 2002 Animation and rendering of complex water surfaces. *ACM Transactions on Graphics (TOG)* **21** (3), 736–744.

Foster, N. & Fedkiw, R. 2001 Practical animation of liquids. In *Proceedings of the 28th annual conference on Computer graphics and interactive techniques*, pp. 23–30. ACM.

Foster, N. & Metaxas, D. 1996 Realistic animation of liquids. *Graphical models and image processing* **58** (5), 471–483.

Gilles, L., Hagness, S. & Vázquez, L. 2000 Comparison between staggered and unstaggered finite-difference time-domain grids for few-cycle temporal optical soliton propagation. *Journal of Computational Physics* **161** (2), 379–400.

Griffiths, D. J. & College, R. 1999 *Introduction to electrodynamics*, , vol. 3. prentice Hall Upper Saddle River, NJ.

Hyman, J. M. & Shashkov, M. 1999 Mimetic discretizations for maxwell's equations. *Journal of Computational Physics* **151** (2), 881–909.

Jackson, J. D. 1999 *Classical electrodynamics*. John Wiley and sons.

Kim, J. W. & Lee, D. J. 1996 Optimized compact finite difference schemes with maximum resolution. *AIAA journal* **34** (5), 887–893.

Kumar, A. 2004 Isotropic finite-differences. *Journal of Computational Physics* **201** (1), 109–118.

Laney, C. B. 1998 *Computational gasdynamics*. Cambridge University Press.

Lele, S. K. 1992 Compact finite difference schemes with spectral-like resolution. *Journal of Computational Physics* **103** (1), 16–42.

LeVeque, R. J. 2007 *Finite difference methods for ordinary and partial differential equations: steady-state and time-dependent problems*. Siam.

Liu, Y. 1996 Fourier analysis of numerical algorithms for the maxwell equations. *Journal of Computational Physics* **124**, 396–416.

Nguyen, D. Q., Fedkiw, R. & Jensen, H. W. 2002 Physically based modeling and animation of fire. *ACM Transactions on Graphics (TOG)* **21** (3), 721–728.

Panaretos, A. H., Aberle, J. T. & Díaz, R. E. 2007 The effect of the 2-d laplacian operator approximation on the performance of finite-difference time-domain schemes for maxwellâs equations. *Journal of Computational Physics* **227** (1), 513–536.

Patra, M. & Karttunen, M. 2006 Stencils with isotropic discretization error for differential operators. *Numerical Methods for Partial Differential Equations* **22** (4), 936–953.

Ramadugu, R., Thampi, S. P., Adhikari, R., Succi, S. & Ansumali, S. 2013 Lattice differential operators for computational physics. *EPL (Europhysics Letters)* **101** (5), 50006.

Schneider, J. B. 2010 Understanding the finite-difference time-domain method. *Scholl of electrical engineering and computer science Washington State University.– URL: http://www. eecs. wsu. edu/˜ schneidj/ufdtd/(request data: 29.11. 2012)* .

Selle, A., Fedkiw, R., Kim, B., Liu, Y. & Rossignac, J. 2008 An unconditionally stable maccormack method. *Journal of Scientific Computing* **35** (2-3), 350–371.

Succi, S. 2001 *The lattice Boltzmann equation: for fluid dynamics and beyond*. Oxford university press.

Taflove, A. & Hagness, S. C. 2000 *Computational electrodynamics*, , vol. 160. Artech house Boston.

Tam, C. & Kurbatskii, K. 2003 Multi-size-mesh multi-time-step dispersion-relation-preserving scheme for multiple-scales aeroacoustics problems. *International Journal of Computational Fluid Dynamics* **17** (2), 119–132.

Tam, C. K. & Webb, J. C. 1993 Dispersion-relation-preserving finite difference schemes for computational acoustics. *Journal of computational physics* **107** (2), 262–281.

Thampi, S. P., Ansumali, S., Adhikari, R. & Succi, S. 2012 Isotropic discrete laplacian operators from lattice hydrodynamics. *Journal of Computational Physics* .

Trefethen, L. N. 1982 Group velocity in finite difference schemes. *SIAM review* **24**, 113–136.

Trefethen, L. N. 1996 *Finite difference and spectral methods for ordinary and partial differential equations*. Cornell University [Department of Computer Science and Center for Applied Mathematics].

Vichnevetsky, R. & Bowles, J. B. 1982 *Fourier analysis of numerical approximations of hyperbolic equations*, , vol. 5. Siam.

Xie, Z., Chan, C.-H. & Zhang, B. 2002 An explicit fourth-order staggered finite-difference time-domain method for maxwell's equations. *Journal of Computational and Applied Mathematics* **147** (1), 75–98.

Yee, K. 1966 Numerical solution of initial boundary value problems involving maxwell's equations in isotropic media. *Antennas and Propagation, IEEE Transactions on* **14** (3), 302–307.

Yefet, A. & Petropoulos, P. G. 2001 A staggered fourth-order accurate explicit finite difference scheme for the time-domain maxwell's equations. *Journal of Computational Physics* **168** (2), 286–315.

Young, J. L., Gaitonde, D. & Shang, J. 1997 Toward the construction of a fourth-order difference scheme for transient em wave simulation: staggered grid approach. *Antennas and Propagation, IEEE Transactions on* **45** (11), 1573–1580.

Yudistiawan, W. P., Kwak, S. K., Patil, D. & Ansumali, S. 2010 Higher-order galilean-invariant lattice boltzmann model for microflows: Single-component gas. *Physical Review E* **82** (4), 046701.

Zhuang, M. & Chen, R. 1998 Optimized upwind dispersion-relation-preserving finite difference scheme for computational aeroacoustics. *AIAA journal* **36** (11), 2146–2148.

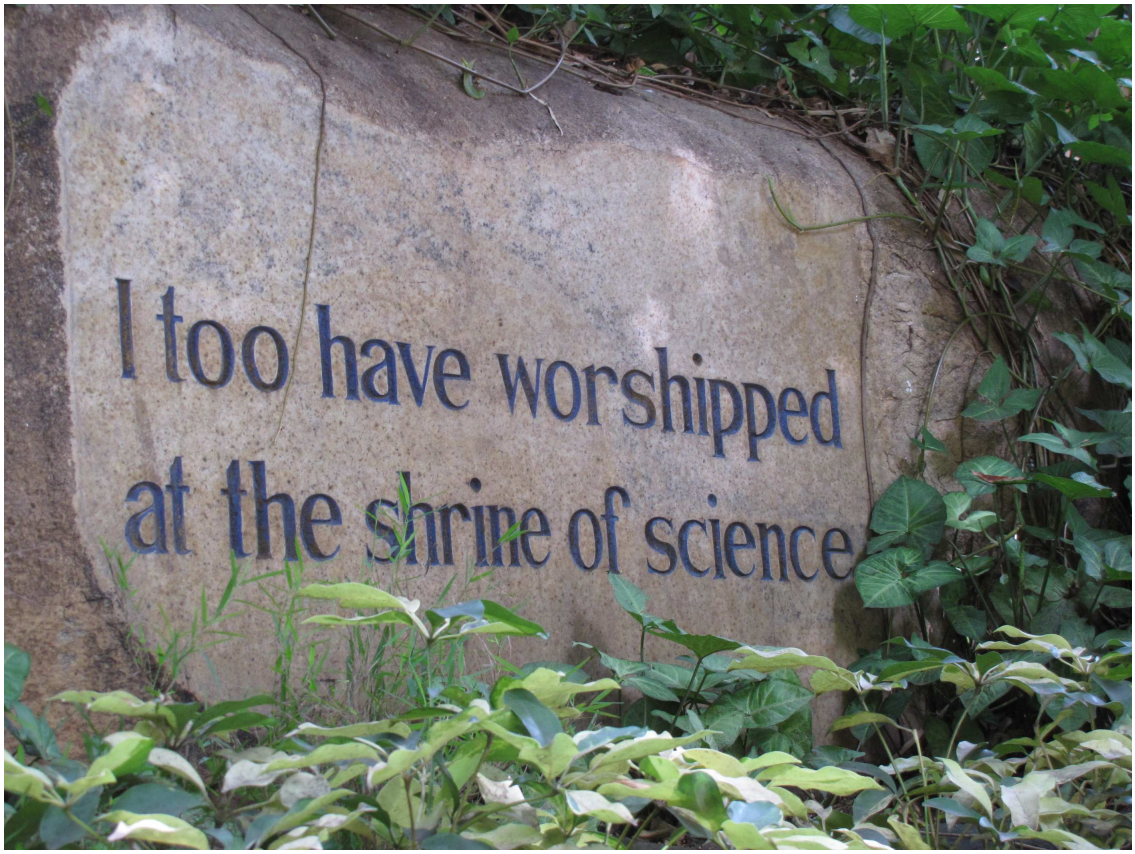
I too have worshipped
at the shrine of science